

# 光学学报

## 臭氧卫星遥感反演进展及挑战

迟雨蕾<sup>1</sup>, 赵传峰<sup>2\*</sup><sup>1</sup> 北京师范大学全球变化与地球系统科学研究院, 北京 100875;<sup>2</sup> 北京大学物理学院大气与海洋科学系, 北京 100871

**摘要** 臭氧是大气中重要的痕量气体, 可影响对流层与平流层大气状态和过程。约 90% 的臭氧集中在平流层, 可吸收下行紫外太阳辐射, 保护地球生命系统; 约 10% 的臭氧位于对流层, 其空间分布多受局地生成和跨区域输送的影响。目前, 臭氧已逐渐成为我国甚至全球首要污染物, 臭氧污染防治也相应地成为我国未来大气污染防治的重点。本文回顾了卫星遥感臭氧的发展进程, 包括臭氧卫星探测传感器、反演算法和应用进展, 并着重分析了臭氧污染相关内容, 包括臭氧污染时空特征分析、典型污染事件分析、臭氧污染与气象条件相互作用等。多种卫星探测载荷的仪器设计和反演技术的不断发展, 使得卫星遥感臭氧反演和监测应用成为可能。卫星可通过紫外谱段和红外谱段而获取臭氧整层信息和垂直分布信息, 目前臭氧柱总量监测精度较高, 但对流层下层和近地面臭氧浓度反演精度还有待提高。根据现阶段的技术水平, 可采用多种技术方法相结合来提升中低层臭氧的探测能力。臭氧污染的监管和防控需要摸清来源, 准确评估污染的成因, 可从前体物排放、化学转化、气象影响、三维传输等方面逐步进行解析。此外, 氮氧化物( $\text{NO}_x$ )和挥发性有机物( $\text{VOC}_s$ )的协同减排是我国臭氧治理的根本所在, 也是下一步的重点研究方向。

**关键词** 大气光学; 臭氧; 卫星遥感; 反演算法; 精度验证; 空气质量; 平流层侵入

中图分类号 P407

文献标志码 A

DOI: 10.3788/AOS230583

### 1 引言

臭氧是地球大气中重要的痕量气体, 会影响对流层与平流层之间的大气交换和空气运动<sup>[1-3]</sup>。90% 的臭氧集中分布在平流层, 浓度最高的部分位于 20~25 km 高度处。平流层臭氧可吸收紫外波段辐射而增温, 其浓度垂直分布可影响平流层的温度结构, 进而影响大气环流和地球气候效应<sup>[4-5]</sup>。同时, 平流层臭氧可以滤除具有生物破坏性的紫外线, 保护地球上的人类和其他生物免遭太阳紫外辐射的伤害<sup>[5]</sup>。

对流层臭氧约占大气臭氧总量的 10%, 会间接影响大气化学、空气质量、气候变化等<sup>[6-7]</sup>。虽然对流层臭氧浓度较低, 但其活泼的化学性质会使其随着温度、水汽、风速、风向、位势涡度、太阳辐射和云等相关因子而变化<sup>[8-11]</sup>。同时, 对流层臭氧可降低生态系统的碳同化能力并对全球产生辐射强迫, 进而对气候变化产生重要影响<sup>[12-16]</sup>。此外, 长距离输送<sup>[17]</sup>、平流层与对流层交换<sup>[18]</sup>、洲际传输<sup>[19]</sup>、季节变化<sup>[20]</sup>等大气动力相关过程也会对臭氧产生影响。特别是在动力、热力和化学属性差异较大的平流层与对流层之间, 某些局部地区会由于天气系统的变化而发生短时间的物质交换(STE)。近地面臭氧对人体健康和生态环境影响重

大, 过量的臭氧会对人的眼睛和呼吸系统造成损伤<sup>[21-22]</sup>, 也会造成农作物减产、橡胶材料损伤<sup>[23]</sup>等生态环境问题。随着臭氧污染愈发严重, 臭氧已成为我国夏秋季的首要污染物。

近地面臭氧的主要来源为光化学反应, 其主要前体物为一氧化碳(CO)、氮氧化物( $\text{NO}_x$ )和挥发性有机物( $\text{VOC}_s$ )<sup>[24]</sup>。其中, 臭氧与前体物  $\text{NO}_x$  和  $\text{VOC}_s$  之间存在复杂的非线性关系, 一般在  $\text{NO}_x$  饱和地区(城镇), 臭氧生成多受  $\text{VOC}_s$  控制; 而在  $\text{NO}_x$  较少的地区(郊区), 臭氧生成多受  $\text{NO}_x$  控制<sup>[25]</sup>。众多研究表明, 近地面臭氧浓度还受局部气象条件和区域输送的影响。气温决定臭氧光化学反应速率和植物排放的  $\text{VOC}_s$  浓度<sup>[26]</sup>, 相对湿度影响臭氧光化学反应过程<sup>[27]</sup>, 风速和风向则影响近地面臭氧扩散与区域传输<sup>[28]</sup>。此外, 臭氧在边界层大气中的寿命较短, 多依赖于太阳辐射强度和其前体物浓度。因此, 可以根据臭氧前体物的时空分布变化进行相对精准的污染防控<sup>[29-30]</sup>。

从臭氧数据的获取方式来看, 地基观测站点可提供精度较高的近地面臭氧的时空分布信息, 其数据稳定性好且具有较好的延续性<sup>[31-32]</sup>, 但站点分布不均匀, 空间代表性较差<sup>[33]</sup>。探空观测和机载观测可提供臭氧的垂直分布及变化趋势, 但缺乏时空连续性, 很难获取

收稿日期: 2023-02-22; 修回日期: 2023-04-27; 录用日期: 2023-05-16; 网络首发日期: 2023-05-26

基金项目: 中国气象局风云卫星应用先行计划(FY-APP-2022.0506)

通信作者: \*cfzhao@pku.edu.cn

大区域范围的臭氧分布。而星载观测可获取全天候的全球臭氧信息,国际上已基于紫外和热红外光谱开发了多种卫星遥感臭氧反演算法(臭氧柱总量反演和臭氧廓线反演)<sup>[34-37]</sup>,也有不少研究尝试对前体物[NO<sub>x</sub>、甲醛(HCHO)]进行监测。通过分析研究臭氧在大气化学过程中的演化过程,可更好地进行空气质量管理<sup>[38-40]</sup>。目前,臭氧柱总量和对流层浓度反演相对较为成熟,精度分别可达95%和85%<sup>[41]</sup>,而受大气气象条件和卫星时空分辨率等要素影响,臭氧廓线和近地面臭氧浓度的反演精度较低,限制了基于卫星观测对近地面臭氧及其影响的研究。

中国地区的臭氧污染近年来愈加严重,多个城市出现呈上升趋势的高浓度臭氧,尤其在夏、秋季<sup>[42-43]</sup>。除了京津冀、珠三角和长三角等人口密集、经济和工业发达的城市地区,近地面高浓度臭氧也频繁出现在其他区域<sup>[44-45]</sup>。我国多采用地面和探空测量来获取臭氧观测信息。近年,我国发射了多个自主研发的单星观测卫星载荷,但缺乏基于卫星载

荷的相对系统性的臭氧反演和研究。我国近地面臭氧污染成因复杂,影响因素较多,基于卫星数据和其他观测数据的协同处理和分析开展臭氧和颗粒物的协同治理是我国下一步大气污染治理的关键<sup>[46-47]</sup>。分析近年来中国近地面臭氧浓度的时空分布特征,了解污染现状,探究其主要影响因素,对我国臭氧污染防治具有十分重要的意义。本文主要从臭氧卫星遥感传感器的发展进程、臭氧卫星遥感的反演算法、应用进展、存在问题和发展趋势等多个方面综合概述臭氧卫星遥感反演。

## 2 臭氧卫星探测传感器的发展

自1960年以来,以美国、中国、俄罗斯为首的多个国家发射了80多颗可用于臭氧相关观测的航天器和卫星,其观测方式逐步从单一卫星向全球同步轨道(TEMPO、Sentinel-4)和协同轨道星座(如A-Train)发展,且卫星探测传感器也变得更为丰富。具体的重要卫星探测传感器将在本节具体介绍。

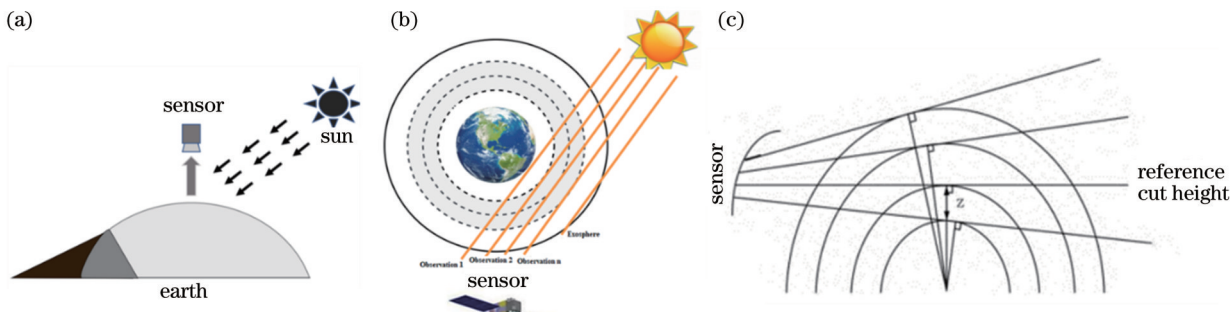


图1 臭氧卫星遥感探测技术的示意图<sup>[65]</sup>。(a) 天底观测;(b) 掩星观测;(c) 临边观测

Fig. 1 Schematic diagram of ozone satellite remote sensing detection technology<sup>[65]</sup>. (a) Nadir observation; (b) occultation observations; (c) limb-viewing

如图1所示,全球臭氧探测仪器主要分为三种探测方式:天底观测;掩星观测;临边观测。天底观测可获取较高精度的臭氧柱总量信息,但获取臭氧廓线的分辨率较低;临边观测可进行多谱段探测(紫外、红外和微波),采样频率和垂直分辨率均较高;掩星观测虽然采样频率较低,但可获取高精度和高垂直分辨率的臭氧廓线。从探测谱段和探测原理来划分,全球臭氧探测仪器可分为紫外光谱探测传感器和红外光谱探测传感器。下面对目前常用的臭氧探测卫星(在轨的紫外传感器和红外传感器)进行详细介绍(图2)。

### 2.1 紫外光谱探测传感器

从臭氧卫星遥感原理分析,紫外光谱探测传感器利用太阳紫外谱段的后向散射辐射信息来监测大气中臭氧浓度,可获取整层臭氧柱浓度和臭氧廓线信息。相对于低层臭氧,整层臭氧柱浓度和平流层臭氧廓线的反演精度较高。其中臭氧廓线反演主要利用大气臭氧对遥感传感器不同波谱的选择吸收差异性来实现大气臭氧的垂直向信息获取。通常只有波长大于

290 nm的波谱辐射可深入对流层,而对流层中大量的云和气溶胶大粒子会通过散射对辐射造成显著影响,因此,利用紫外光谱探测传感器反演的对流层臭氧廓线精度会受限。

近年来国际上已发射了众多用于臭氧卫星探测的紫外传感器。全球臭氧监测实验仪器(GOME)搭载于欧洲航天局(ESA)在1995年发射的ERS-2卫星上,该仪器以0.2~2.4 nm的分辨率来测量240~790 nm光谱范围内的大气后向散射辐射,并获取臭氧、HCHO和乙二醛(CHOCHO)等痕量气体廓线数据<sup>[36]</sup>。GOME-2于2012年9月搭载于Metop-A卫星发射。除继承GOME(空间分辨率为40 km×320 km,时间分辨率为3 d)的优势外,GOME-2将空间分辨率提高到40 km×80 km,且1.5 d可覆盖全球<sup>[48]</sup>。2002年搭载于ENVISAT卫星发射的SCIAMACHY传感器,具有三种探测方式,其光谱覆盖范围广(240~2400 nm),可获取微量气体、云和气溶胶的分布情况,该传感器于2012年结束服役<sup>[49-50]</sup>。臭氧检测仪(OMI)

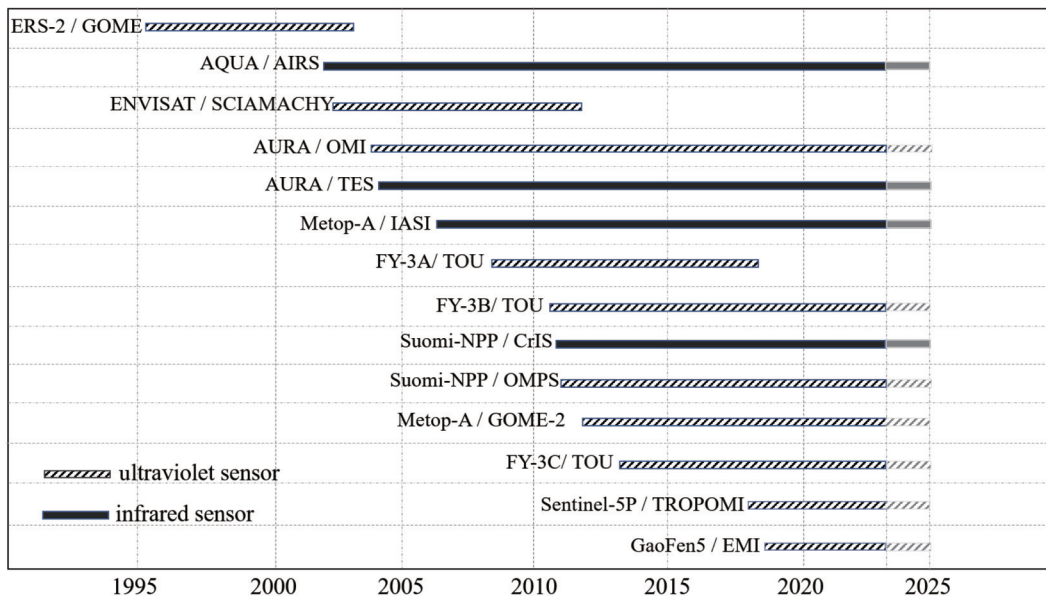


图2 主要的臭氧卫星探测传感器(紫外传感器和红外传感器)

Fig. 2 Main ozone satellite detection sensors (ultraviolet sensors and infrared sensors)

搭载于EOS-Aura卫星于2004年发射,它继承了GOME和SCIAMACHY等仪器的特点,提高了空间分辨率和全球连续覆盖度<sup>[51]</sup>,并利用臭氧总量绘图分光仪(TOMS)和差分光学吸收光谱(DOAS)算法实现了空间分辨率为13 km×24 km的全球臭氧总量、对流层臭氧柱总量和臭氧廓线反演。同时,OMI是目前为止服役时间最长的臭氧传感器,所获取的数据连贯性最好。搭载于Suomi NPP卫星上的臭氧成像探测仪(OMPS)于2011年8月发射,其天底观测可覆盖整个测量光谱范围,具有较高的信噪比,可每天提供连续的全球性臭氧产品<sup>[52-53]</sup>。该传感器避免了行异常问题,数据质量高。搭载于2017年ESA发射的Sentinel-5P极轨卫星上的对流层监测光谱仪TROPOMI,与其他在轨卫星相比具有最高的空间分辨率(3.5 km×7 km),可有效地观测全球痕量气体组分,包括臭氧、NO<sub>2</sub>、SO<sub>2</sub>、HCHO、CH<sub>4</sub>和CO等与人类活动密切相关的重要组分,同时加强了对气溶胶和云的观测<sup>[54-55]</sup>。大气痕量气体差分吸收光谱仪(EMI)搭载于我国高分5号卫星和高光谱观测卫星,可实现对臭氧、NO<sub>2</sub>、SO<sub>2</sub>和CH<sub>4</sub>等痕量气体的定量监测和变化分析<sup>[56-58]</sup>。

此外,风云系列臭氧卫星(FY-3)也可获取大气中的臭氧数据,实现全球气候变化和大气环境污染等监测和研究。我国第二代极轨气象卫星风云三号[FY-3A(2008年5月)、FY-3B(2010年11月)和FY-3C(2013年9月)]均搭载了臭氧成像光谱仪(OMS)、紫外臭氧总量探测仪(TOU)和太阳后向散射紫外仪(SBUS),可获取全球的臭氧总量和臭氧廓线,从根本上改变了我国大气臭氧探测和研究的现状。TOU和SBUS是我国首次自主研制的星载卫星紫外臭氧观测仪,可用于获取全球臭氧总量和垂直分布变化。上述

在轨卫星的具体参数见表1。

## 2.2 红外光谱探测传感器

红外光谱探测传感器通常利用臭氧在9.6 μm吸收带的热辐射信息来获取臭氧在大气中的垂直分布和浓度信息,它们多采用高分辨率、高灵敏度的光学元件和探测器,因此,可获取垂直分辨率较高的臭氧廓线信息。但在反演过程中,由于温湿廓线误差会对辐射量和臭氧权重函数的计算产生较大影响,基于红外光谱探测传感器的对流层臭氧廓线反演具有一定的不确定性。目前,热红外高光谱测量仪器多采用临边观测的探测方式,常用的仪器包括温室气体干涉测量仪(IMG)<sup>[59]</sup>、大气红外探测器(AIRS)<sup>[60]</sup>、对流层发射光谱仪(TES)<sup>[61]</sup>、红外大气探测干涉仪(IASI)<sup>[62-63]</sup>和交叉轨道红外探测器(CrIS)<sup>[64]</sup>等,可全天候连续测量地球大气临边所发出的长波辐射,具有更广的覆盖范围,很好地弥补了天底观测无法获取高分辨率的中高层痕量气体廓线的问题<sup>[65]</sup>。

搭载于对地观测卫星ADEOS上的IMG于1996年8月发射,光谱区间是3.3~15 μm,是国际上首个采用天底观测方式进行臭氧探测的星载高光谱傅里叶光谱仪<sup>[59]</sup>。AIRS由美国国家航空航天局(NASA)和喷气推进实验室(JPL)联合开发并于2002年5月搭载AQUA卫星发射,拥有2378个连续红外光谱通道(3.7~15.4 μm),可用于对地球大气层中的温度、湿度、云层特性、大气成分(臭氧、气溶胶和二氧化碳等)的垂直分布进行精密观测<sup>[60]</sup>。TES是搭载在NASA AURA卫星上的一种臭氧红外传感器,光谱覆盖范围为3.2~15.4 μm,用于测量大气中的臭氧和其他气体的分布和浓度,尤其是对对流层和平流层中臭氧垂直分布进行高分辨率探测<sup>[61]</sup>。IASI是搭载于METOP

表1 常用臭氧探测卫星传感器的具体参数  
Table 1 Specific parameters of commonly used satellite sensors for ozone detection

Sensor	Satellite platform	Research institution	Satellite transit time	Temporal resolution /d	Spatial resolution / km	Spectra range / $\mu\text{m}$	Service period
GOME	ERS-2	ESA	10:30	3	40×320	0.24–0.79	1995–2003
GOME-2	METOP-A	ESA	9:30	1.5	40×80	0.25–0.79	2012–2023
SCIAMACHY	ENVISAT	ESA	10:00	6	30×60	0.24–2.40	2002–2012
OMI	AURA	NASA	13:45	1	13×24	0.27–0.50	2004–2023
OMPS	Suomi-NPP	NASA	13:30	1	50×50	0.25–0.42	2011–2023
EMI	GaoFen5	China	13:30	1	13×48	0.3–0.5	2018–2023
TROPOMI	Sentinel-5P	ESA	13:30	1	3.5×5.5	0.27–0.32, 0.310–0.495, 0.675–0.775, 2.305–2.385	2017–2023
TOU	FY-3A FY-3B FY-3C	China Meteorological Administration	13:40	1	50×50	0.30–0.36	2008–2018 2010–2023 2013–2023
AIRS	AQUA	NOAA	13:30	1	14×14	3.74–15.4	2002–2023
CrIS	Suomi-NPP	NASA	13:30	1	14×14	3.9–15.4	2011–2023
TES	AURA	NOAA	13:45	16	0.5×5	3.3–15.4	2004–2023
IASI	Metop-A	ESA	21:30	1.5	80×40	3.63–15.50	2006–2023

卫星上的臭氧红外传感器,可测量地球系统发射的低空红外光谱,其光谱范围为3.63~15.50  $\mu\text{m}$ ,提供大气中水汽、温度、气压等气象要素的垂直分布信息和臭氧总量及其垂直分布<sup>[62–63]</sup>。CrIS是由美国NASA和美国国家海洋和大气管理局(NOAA)合作开发的卫星遥感传感器,其主要通过探测地球大气层顶部向上辐射的红外辐射来获取大气垂直廓线的信息,其中测量大气成分(臭氧)的波段为9.94~14.26  $\mu\text{m}$ <sup>[64]</sup>。CrIS具有高空间分辨率(14 km×14 km),可提供高精度的臭氧垂直廓线信息。上述在轨卫星的具体参数见表1。

### 3 臭氧卫星遥感算法进展

目前,臭氧卫星遥感反演方法主要分为两大类,分别是臭氧柱总量反演和臭氧廓线反演方法。基于星载臭氧数据,融合多源数据可估算近地面臭氧浓度信息。上述各类算法的进展和应用在本章中详细介绍。

#### 3.1 臭氧柱总量反演算法

常用的臭氧柱总量获取方法主要有四类,分别为比值法、紫外后向散射(BUV)法、DOAS法和产品合成法。各反演算法均比较成熟,精度可达90%,具体的算法特点和应用见图3。其中,UVB和DOAS算法是紫外臭氧总量反演的常用算法。UVB算法通常遵循两个假设:假设云为不透明的朗伯反射体,且云顶有效反照率不随波长的变化而变化;假设探测波长处的后向散射强度只与大气臭氧总量有关,而与臭氧廓线

无关。早期,Dave等<sup>[34]</sup>利用310 nm波长附近的后向散射获取大气臭氧总量。针对Nimbus-7卫星,算法经过改进后形成V7和V8算法。Wellemeier等<sup>[65]</sup>和Balis等<sup>[67]</sup>的研究表明,TOMS-V8算法通过对气溶胶散射作用进行校正,并且采用多组波长数据进行臭氧总量迭代计算来降低仪器噪声误差,可以有效提高反演精度,具有更强的臭氧分布信息表达能力。

与TOMS算法相比,DOAS算法采用更长的波长来获取臭氧总量,且对气溶胶吸收和误差校正所引起的干扰效应具有较低的敏感性,因此,DOAS算法可使用不同的光谱窗口来最小化臭氧分布的相关误差。针对DOAS算法在高纬度地区反演GOME数据而出现的高估问题,Coldewey-Egbers等<sup>[36]</sup>采用加权函数形成WFM-DOAS方法,该方法考虑了观测较大太阳天顶角而产生的波长依赖性,消除其对大气质量因子(AMF)转换的影响,进而改善了拟合残差。Ebojje等<sup>[49]</sup>将DOAS算法应用于SCIAMACHY数据来反演臭氧柱总量,可很好地表达臭氧的季节性变化。同时,将反演结果与探空数据进行对比发现,验证结果吻合度较高(<3 DU)。此外,TROPOMI传感器的官方臭氧柱总量产品也采用了DOAS算法,Garane等<sup>[54]</sup>利用世界臭氧和紫外线辐射数据中心(WOUDC)站点数据验证TROPOMI臭氧柱总量产品,发现平均偏差为0%~1.5%。

产品合成法多在UVB和DOAS算法的基础上开展。张莹等<sup>[68]</sup>基于TOMS、OMI、FY-3A的TOU臭氧

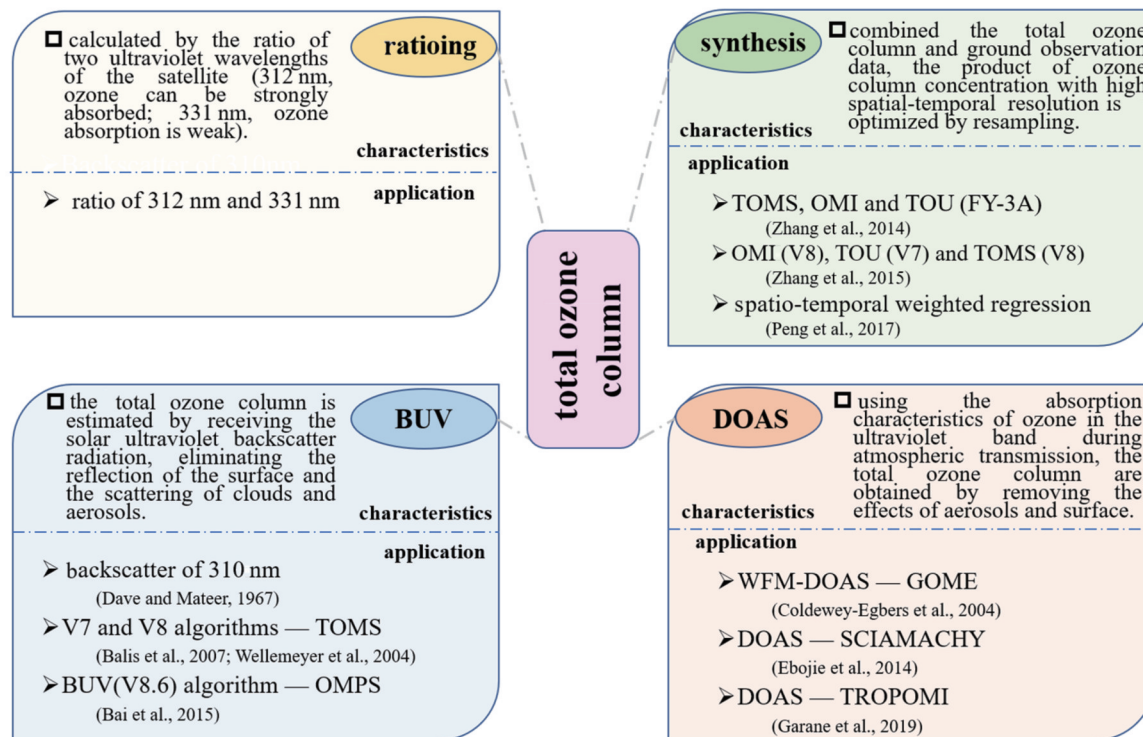


图3 臭氧柱总量反演算法详解

Fig. 3 Detailed explanation of retrieval algorithm for total ozone column

总量产品,利用最邻近采样方法生成一套近30年的空间分辨率为 $0.25^\circ \times 0.25^\circ$ 的数据集,并以WOUDC地面站数据对OMI和TOU数据进行回归分析以订正反演产品,发现2000年后中国上空臭氧下降速率减缓,2005年后总量上升趋势与全球趋势一致。张艳等<sup>[69]</sup>将OMI、FY-3 TOU和TOMS的反演产品进行插值而获得1979—2014年间的臭氧总量数据,发现中高纬度地区臭氧具有不均匀性,特别是青藏高原的臭氧增长高于同纬度其他地区。针对OMI卫星在赤道地区的条带缺失问题,彭晓琳<sup>[70]</sup>基于时空加权回归方法构建目标数据与多时相辅助数据的时空关系模型,实现了全球OMI臭氧总量产品全覆盖,生成一套2004—2014年时空连续的全球臭氧总量日产品。

### 3.2 臭氧廓线反演算法

大气臭氧廓线反演算法包含三个核心点,分别是不同大气敏感通道的选取、分析太阳辐射与不同大气分层之间的相互作用、引入对复杂的多元非线性物理模型的求解方法和大量可靠的先验信息。其中选取合适的辐射传输模型是三个核心点的关键,目前最常用的方法包含基于贝叶斯理论的最优估计法和特征向量法。Rodgers<sup>[71]</sup>最早提出针对正向大气模式最优估计法的理论框架,借助先验信息约束模型的解,利用最大似然估计来迭代求解,此方法至今被广泛应用于臭氧廓线反演算法。最优化反演的求解过程从数学方程意义上可以拥有多个正确解,需采用合理的约束条件(反演初始廓线的选择、优化方法的选择等)来确定高

精度和强稳定性的反演结果。初始廓线的选择是大气臭氧廓线反演中的重要约束条件,可采用统计回归方法、模式计算、气候资料取平均等三种方式进行获取。统计回归方法多依赖于廓线样本的精度;模式计算方法的垂直分辨率和稳定性较低;气候资料取平均方法的观测资料有限,直接影响初始廓线的精度。

自1970年开始,在德国、美国、日本和南极地区均有开展常规臭氧探空廓线监测;而船载监测发展于20世纪70年代后期,多出现在北大西洋和南大西洋边界层<sup>[29]</sup>。发展至今,全球已具有充足的臭氧廓线数据。臭氧廓线反演可基于紫外传感器和热红外传感器进行,图4介绍了近年来臭氧廓线反演的主要传感器及其应用。SBUV和SBUV/2传感器提供了近40年的全球臭氧廓线数据,Bhartia等<sup>[72-73]</sup>先后介绍了V6和V8算法,并利用平滑内核比较SBUV数据与微波边缘测深仪(MLS)臭氧廓线,发现其在平流层下层位置具有较大作用,SBUV臭氧廓线的垂直分辨率略低于MLS。Petropavlovskikh等<sup>[35]</sup>提出了一种新的Umkehr臭氧廓线反演算法,该算法可研究月均距平的长期变化,在不受先验信息影响的基础上评估多年时间序列的气候变异性,在平流层中的不确定性低于5%。Huang等<sup>[74]</sup>介绍了FY-3卫星紫外臭氧垂直廓线反演算法FY-V1.0,并与SBUV和SBUV/2的臭氧廓线进行了比较,结果表明,FY-3卫星臭氧廓线反演精度较高,与SBUV和SBUV/2的臭氧廓线的平均相对误差在 $\pm 7\%$ 以内。黄富祥等<sup>[75]</sup>还将FY-3卫星臭氧廓线

与美国NOAA V8业务反演产品比较,发现吻合度较好,相对反演精度在±2%以内。臭氧廓线反演算法OPERA可应用于GOME、GOME-2和OMI等传感器,Van Peet等<sup>[48]</sup>描述了OPERA算法的详细设置,并将GOME和GOME-2的臭氧廓线反演结果与臭氧探测结果进行全球比较,结果表明,对流层的相对差异为20%,平流层的相对差异为15%,满足ESA气候变化倡议(CCI)项目用户要求规定。Miles等<sup>[76]</sup>重点评估了GOME-2对流层臭氧廓线的性能,结果表明,在应用反演垂直平滑(平均核)的基础上,对流层下部的反演偏差可达6%(1.5 DU),精度较高。OMPS传感器同时提供了臭氧柱总量和臭氧廓线的反演值。Flynn等<sup>[77]</sup>详细介绍了OMPS传感器的工作原理和反演方法,并对臭氧反演产品进行初步评估,发现平流层中上层的臭氧廓线的偏差通常在±5%范围内。Arosio等<sup>[78]</sup>将OMPS臭氧廓线反演结果与MLS数据进行对比,结果表明,20~60 km的OMPS臭氧廓线与MLS V4.2数据的差异性在5%~10%的范围内,而在较低的海拔范围内,偏差变得更大,尤其是在热带地区。针对OMI传感器,刘诚<sup>[79]</sup>提出了一种卫星遥感大气臭氧廓线的反演算法,主要利用OMI紫外辐射光谱数据,计算辐射光谱模拟值和权重函数参数,基于最优估计技术反演地表至60 km大气臭氧廓线信息。Kroon等<sup>[80]</sup>将OMI臭氧廓线与MLS和TES的臭氧廓线进行比较,结果表明,OMI平流层臭氧廓线与全球相关数

据的一致性在20%以内,但春季的局部极地地区除外;OMI的对流层臭氧廓线在热带和中纬度地区,分别有60%和30%的数据出现系统正偏差。Bak等<sup>[81]</sup>研究了基于对流层顶(TB)的臭氧气候学在OMI臭氧廓线反演中的应用,发现其会提升热带和温带臭氧垂直廓线的反演能力。2021年,德国不来梅大学环境物理研究所开发了TOPAS算法,用于从天底观测的星载传感器中反演臭氧垂直廓线,并应用于TROPOMI L1B光谱数据(270~329 nm)。Mettig等<sup>[55]</sup>利用臭氧激光雷达数据、MLS数据和OMPS数据验证了TROPOMI传感器TOPAS算法反演的臭氧廓线,发现臭氧激光雷达数据与TROPOMI反演结果显示非常好的一致性,18~45 km的相对平均偏差在±5%以下,标准差为10%。MLS和OMPS的臭氧廓线与TROPOMI反演结果一致性较高,除极地高纬地区外,20~50 km的相对平均差基本在±5%以下。Zhao等<sup>[37]</sup>利用TROPOMI反演的臭氧廓线,结合NO<sub>x</sub>和HCHO的对流层垂直柱密度评估了中国新冠肺炎暴发期间对流层臭氧的变化,结果表明,在封控期间华东地区的总有机碳增加了10%,而臭氧的产生并没有显著减少。这主要是由于NO<sub>x</sub>排放的减少削弱了臭氧滴定作用,导致臭氧增加。综上所述,紫外散射光谱易受气溶胶和地表反射率等要素的影响,且臭氧吸收线在紫外波段不受高度和压强的影响,基于紫外传感器的对流层臭氧廓线的反演精度较低。

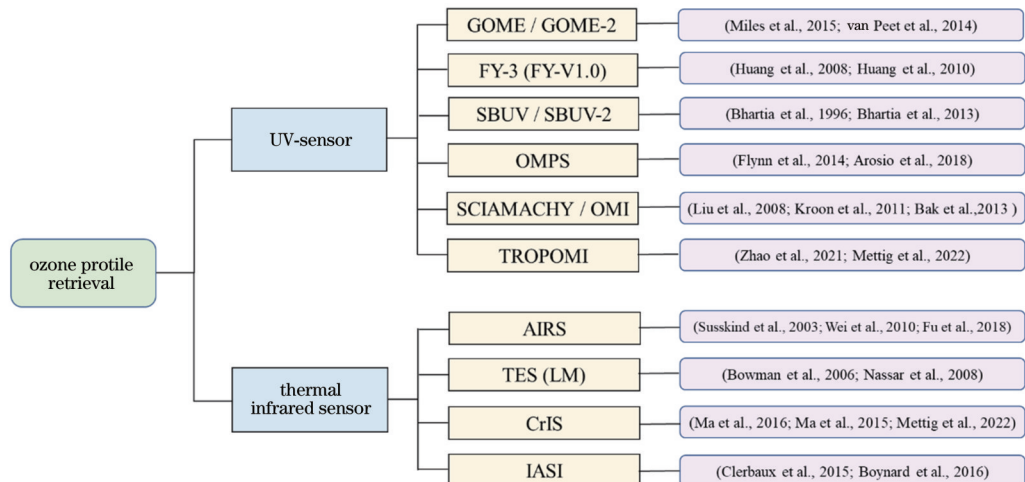


图4 近年来臭氧廓线反演的主要传感器及应用

Fig. 4 Main sensors and applications of ozone profile retrieval in recent years

针对臭氧吸收线在红外波段随温度和压强而变化这一原理,热红外臭氧吸收波段可用于反演臭氧廓线(图4)。Susskind等<sup>[82]</sup>采用最优化估计法对AIRS传感器的41个通道(9.6 μm臭氧吸收波段)反演臭氧廓线,并采取业务化处理。Wei等<sup>[83]</sup>采用最优化估计法的同时,通过调整先验廓线来提高AIRS臭氧廓线的反演精度,调整后中纬度地区总的自由度可达1.1~2.5。针对TES传感器,Bowman等<sup>[84]</sup>采用具有强约

束的Levenberg-Marquardt(LM)方法来反演臭氧廓线,经过验证表明,对流层上部臭氧廓线反演误差最小,但易受平流层下层臭氧的影响。同时,Nassar等<sup>[61]</sup>将TES V2.0臭氧廓线产品与全球臭氧探空数据进行对比验证,结果表明,TES V2.0臭氧廓线产品在对流层内的误差小于10 ppb(十亿分比浓度,也即在溶液中用溶质质量占全部溶液质量的十亿分比来表示的浓度)。Ma等<sup>[64]</sup>着重分析了臭氧吸收光谱和权重函数对

温度的敏感性及其对臭氧廓线反演的影响,经过实验发现,CrIS在平流层中上层对臭氧敏感,在10~100 hPa之间的垂直敏感性达到峰值,由1 K温度变化而产生的权重函数变化与臭氧廓线6%的变化一致。此外,他们还将臭氧廓线数据与探空数据进行对比分析,结果表明,CrIS平流层、对流层高层和对流层中层的臭氧廓线的反演误差分别在10%、5%和30%以内,且400 hPa以下的臭氧廓线多来自于先验廓线。IASI传感器的臭氧廓线也是基于最优估计法而反演的,Clerbaux等<sup>[62]</sup>发现IASI对6~8 km的对流层臭氧比较敏感,特别是当地表与其上方大气之间存在较大的温度差时,臭氧廓线的敏感性会增加。Boynard等<sup>[63]</sup>将IASI臭氧廓线与WOUUDC数据进行对比验证,结果表明,IASI对流层臭氧廓线低估了5%~15%。综上所述,热红外传感器对对流层中上层的臭氧比较敏感,廓线反演精度较高,而对流层中下层臭氧廓线反演多依赖于先验廓线,反演精度较低。同时,温度和水汽会对热红外臭氧吸收波段产生影响,进而增加不确定性。

目前,臭氧廓线反演算法多受卫星数据质量、云辐射和反演方法等因素的影响,反演精度多在70%~75%左右。紫外传感器与红外传感器的结合可提高对流层中低层臭氧的反演精度。Worden等<sup>[85]</sup>利用TES、OMI和TES+OMI传感器组合的方式,联合紫外和红外波段反演臭氧廓线,结果表明,边界层臭氧廓线精度提高2倍以上,且对流层臭氧廓线的垂直分辨率比TES的垂直分辨率提高20%~60%。Natraj等<sup>[86]</sup>探索了紫外至热红外波谱对对流层臭氧边界的敏感性,发现紫外+可见光、紫外+热红外,以及紫外+可见光+热红外结合可以满足观测对流层臭氧的要求。简单的联合反演并不能消除红外波段温度误差带来的不确定性。Zhang等<sup>[87]</sup>结合紫外和红外谱段臭氧探测优势,利用OMPS臭氧总量作为约束条件,反演CrIS/Suomi-NPP的对流层臭氧廓线,并将反演结果与探空数据和激光雷达观测数据进行对比验证,结果表明,经过OMPS臭氧柱总量约束的反演相对误差小于未经约束的反演相对误差,且平均核函数的峰值增大了约1倍。

对流层臭氧反演一直是臭氧卫星探测的一个难点,除精确的对流层臭氧廓线反演算法外,还可以借助某些辅助信息,在计算臭氧总量的基础上计算对流层臭氧柱浓度,常用方法是余值法<sup>[88-91]</sup>、扫描角几何法<sup>[92]</sup>和对流云微分法<sup>[93]</sup>。Fishman等<sup>[88]</sup>最早采用余值法计算对流层臭氧。他假设平流层臭氧在一定空间范围内为恒定值,特别是在热带地区180°经线附近的海洋上。基于此,对流层臭氧可用TOMS测量的臭氧总量减去SAGE仪器测量的平流层臭氧浓度而获得。之后, Kim等<sup>[80-90]</sup>对余值法进行了改进,在城市地表类型下或具有生物燃烧的地区,引入有效因子来提高对流层臭氧的估算精度。近年,Schoeberl等<sup>[91]</sup>采用前向轨迹

模型来优化余值法,不仅提高了MLS传感器对流层臭氧产品的水平分辨率,更提高了对流层臭氧产品在热带和中纬度地区的估算精度。

### 3.3 基于多源数据的近地面臭氧估算方法

近地面高浓度臭氧会对人类生产生活产生重大影响,其获取方式主要包括地基站点观测和机载观测,这两种方式难以获取较大空间覆盖范围内高精度的近地面臭氧浓度。然而星载传感器很难探测到近地面层,难以获取近地面臭氧浓度。同时,影响近地面臭氧的主要因素包括臭氧的前提物(NO<sub>x</sub>、VOC<sub>x</sub>等)、影响臭氧光化学合成的气象条件(太阳辐射和温度等)和影响臭氧传输的气象因素(水平风场和垂直速度等)。针对臭氧浓度和其影响因素之间的复杂关系,国内外众多学者已尝试运用不同模型来估算近地面臭氧浓度。

Cobourn等<sup>[94]</sup>利用肯达基州1998—1999年近地面臭氧浓度观测数据集,以气象预测数据为输入,比对了混合非线性回归(NLR)模型和神经网络(NN)模型对次日最大1 h臭氧平均地面浓度的预测水平,发现两个模型表现基本相同(NLR模型和NN模型的平均绝对误差分别为12.5 ppb和12.3 ppb)。Cannon等<sup>[95]</sup>使用哥伦比亚地区10个监测站的臭氧观测数据建立了预测每日最高小时平均臭氧浓度的经验模型,输入相同的1991—1996年站点臭氧数据,发现神经网络模型的方差比多元线性回归模型的方差减少了约7%,说明神经网络可以有效地构建臭氧估算模型。Chaloulakou等<sup>[96]</sup>利用人工神经网络和多元线性回归模型对雅典盆地的4个监测站的监测数据(11个预测因子)构建模型进行对比研究,预测了次日小时最大臭氧浓度。验证结果显示,人工神经网络能够更好地估算监测点的臭氧浓度,对于臭氧浓度超过阈值的情况预测准确率达到72%。Wang等<sup>[97]</sup>针对人口密集的城市地区所出现的高浓度臭氧情况,将自适应径向基函数(ARBF)网络与特定区域的统计特性相结合,建立了一种改进的神经网络方法,用于预测臭氧的日最大浓度。该研究利用1999—2000年间在香港3个空气污染物监测站收集的小时时间序列数据对改进后的模型进行了训练和验证,结果显示该方法具有有效性和可靠性。

近地面臭氧估算方法近几年发展迅速,算法主要结合多源遥感观测数据进行大样本数据迭代优化,目前常利用机器学习模型和深度学习网络技术。Chattopadhyay等<sup>[98]</sup>使用1932—1971年瑞士每月臭氧柱总量建立数据集,分别对双层感知器和单层感知器模型进行了训练和验证,模型选择S型激活函数并设定模型学习率为0.9。结果显示,双层感知器模型对平均总臭氧月浓度的预测效果比单层感知器效果好,表明多层感知器能够更好地模拟各影响因素和臭氧浓度的关系。为了解决臭氧浓度在线分析仪器在臭氧应用方面的局限性,张海传等<sup>[99]</sup>监测影响臭氧浓度的6

个因素,提出了基于径向基(RBP)神经网络模型对臭氧浓度进行测量的方法,同时结合训练算法(梯度下降算法)来确定径向基函数的中心和获取输出层的权值。实验证明,应用径向基神经网络预测臭氧的浓度与实际仪器测量的结果绝对误差小于 $5\text{ g/m}^3$ 的数据样本达到93%,而绝对误差小于 $1\text{ g/m}^3$ 的数据样本达到33%以上。Luna等<sup>[100]</sup>根据变量排序选择人工神经网络和支持向量回归等非线性回归方法对相同的数据集进行预测验证,结果显示,神经网络和支持向量回归的均方根误差分别为 $7.66\text{ }\mu\text{g/m}^3$ 和 $7.85\text{ }\mu\text{g/m}^3$ 。之后,Taylan<sup>[101]</sup>提出使用自适应神经模糊推理方法(ANFIS)对臭氧浓度进行估算的方法,该方法结合模糊推理和神经元,使用 $\text{NO}_x$ 、大气压力、温度和相对湿度等影响因素来评估模型性能。研究表明,ANFIS改进了神经网络的适应性,并提升了模型的鲁棒性。Gao等<sup>[102]</sup>以9个气象和光化学参数为输入变量训练神经网络,基于蒙特卡罗仿真进行不确定度和灵敏度分析,显示人工神经网络能较好地预测环境臭氧浓度,也说明温度、大气压力、日照时间和最大风速是影响臭氧预测的主要输入变量。

近年来,众多研究人员基于多源数据(例如CTMs输出、气象资料的同化数据、站点数据和臭氧柱浓度遥感观测等)来生成近地面臭氧浓度数据<sup>[33,103-106]</sup>。这些研究多采用机器学习方法来构建多源数据与地基站点测量值之间的经验拟合关系,从而形成经验模型进行近地面臭氧浓度的估算。例如,Liu等<sup>[103]</sup>采用对流层臭氧浓度,结合适当的辅助变量,通过极端梯度提升(XGBoost)的机器学习方法来预测中国每日最大8小时(MDA8)地面臭氧浓度。Zhang等<sup>[104]</sup>基于OMI的 $\text{NO}_2$ 和 $\text{CH}_4$ 数据集,使用地理加权回归(GWR)方法估算了中国东部地区的地面臭氧月浓度。Li等<sup>[105]</sup>提出了随机森林广义加权模型,利用OMI观测的臭氧柱浓度,结合气象变量和地表因素等估算了青藏高原长期地面MDA8臭氧浓度。DeLang等<sup>[106]</sup>通过使用组合方法(M3Fusion和贝叶斯最大熵)对观测和模式模拟进行数据融合,产生了每年10 km精细空间分辨率的全球地面臭氧浓度。Wang等<sup>[107]</sup>利用葵花八号多个热红外波段的亮温来估算除新疆和西藏外的中国2 km/h的地面臭氧浓度,主要模型采用的是基于类别增强的自适应地理空间局部化方案(SGLboost)。上述这些数据融合框架已经取得了宝贵的近地面臭氧浓度的研究成果,并为科学界作出了重要贡献。

## 4 臭氧卫星遥感应用进展

### 4.1 臭氧卫星观测数据的精度验证

考虑到臭氧源、汇和生命周期的非均一性,其浓度具有很大的季节变化和时空差异性,很难用一种科学模式来描绘和解释全球性臭氧趋势和内在联系。目前,地表、探空、航空、航天飞机和卫星观测均可用于卫

星和模式模拟不确定性验证,其中NASA提供了全面的验证数据集。

在卫星观测的连续性和大尺度性与科学研究算法准确性的共同推动下,卫星反演臭氧柱浓度和臭氧垂直廓线的精度也越来越高,选择精度验证的方式也呈现出多元化。[表2](#)展现了卫星臭氧观测数据精度验证的应用分析案例,从中可以发现卫星数据之间的相互印证、探空数据和地基站点臭氧数据的验证是最常用的方式。近年来近地面臭氧污染成因、臭氧空洞恢复等科学问题愈发被关注,但近地面臭氧浓度的高精度反演和平流层臭氧侵入对近地面臭氧的影响量化等工作仍是研究的焦点问题。

### 4.2 臭氧污染相关研究

臭氧污染主要是指在距地球表面10 km范围高浓度臭氧对环境和人类健康产生的负面影响。对流层中下层臭氧和近地面臭氧是臭氧污染的主要构成。基于卫星的对流层臭氧反演数据和近地面臭氧估算结果是臭氧污染分析研究的核心数据源。

#### 4.2.1 臭氧污染时空特征分析

低层大气中的臭氧主要是由人类活动中排放的 $\text{NO}_x$ 、 $\text{VOC}_s$ 和 $\text{CO}$ 等前体物在特定的气象条件下经过一系列复杂的光化学反应生成的。研究近地面臭氧的变化和时空分布特征,对城市空气质量的改善、理解和应对气候变化、生态保护和农业生产等都有非常重要的作用。

臭氧数据集可以用于分析典型区域的近地面臭氧空间分布特征,并可以结合《环境空气质量标准》,详细地刻画轻度、中度和重度臭氧污染的位置和分布。同时,基于臭氧空间分布特征还可以分析重污染地区臭氧浓度高值的影响因素,并研究各影响因素的时间变化特征。Wu等<sup>[117]</sup>采用2013—2017年的OMI数据计算了中国地区的年均臭氧对流层柱浓度的空间分布,分析了臭氧空间分布与其前体物因子的相关性。蒙特卡罗分析表明,估算的臭氧形成潜能(OFP)与对流层臭氧柱浓度在99.9%的置信区间显著相关。Fan等<sup>[42]</sup>基于国家空气质量地面观测网络在2014年5月至2018年12月期间的300多个城市的站点观测数据,系统分析和揭示了中国7个区域的空气污染特征和时空变化趋势,发现臭氧最大每日8小时平均值( $\text{O}_3\text{MDA }8$ )正在以平均每年4.6%的速度持续增加。这进一步说明臭氧污染成为继颗粒物后大家普遍关注的焦点污染问题,也使得研发臭氧浓度的遥感卫星反演方法,获取覆盖广、质量高的近地面臭氧浓度,变得尤为迫切。

臭氧的时间变化特征是研究和分析臭氧污染的另一个重要途径,包括年际变化、季节变化、月际变化和日变化等。年际变化和季节变化特征可以清晰地说明某一区域臭氧的季节变化特点,而日变化特征的规律性跟当地辐射、云、气溶胶和排放信息的日变化特征紧密联系,可以用于分析各个因子的臭氧污染相对贡献。

表2 卫星臭氧观测数据的精度验证应用分析  
Table 2 Application analysis of accuracy verification of satellite ozone observation data

Source of validation data	Application analysis
Surface	Bian et al <sup>[108]</sup> used observation data of Dobson and TOMS to analyze the long-term trend of total ozone in Beijing and Kunming from 1979 to 2000, and found that the two data had high consistency in the measurement of total ozone. Chen et al <sup>[109]</sup> analyzed the ozone concentration from ground-based stations and TOMS ozone observation data in Shanghai. The results show that their trends are similar (correlation coefficient is 0.81), but the ground-based results are lower than the results of TOMS data.
	Hong et al <sup>[110]</sup> compared and analyzed the total column ozone obtained from OMI-DOAS algorithm with ground-based observations in Seoul, and found that the seasonal average of ground-based observations was underestimated by 2.68%.
Radiosonde	Cai et al <sup>[111]</sup> used ozone sounding data to verify the ozone profile and tropospheric ozone column concentration of GOME satellite in Lhasa, Xining and Beijing. The results show that the monthly average ozone concentration in the lowest layer (0-2.5 km) of the GOME satellite has a good correlation with the ground observations. In addition, the average deviation of the tropospheric column concentration is within 10%. At Zhongshan Station, Amundsen-cott South Pole Station and Neumayer Station, Zhang <sup>[112]</sup> verified the correlation between the data of ozone sounding and the ozone vertical profile of the sixth edition of AIRS in 2008, and found that the two data showed similar trends after analysis.
Satellite observation	Chen et al <sup>[113]</sup> verified OMPS ozone profile using ozone sonde data from 2016 to 2018 in Beijing. The results show that the relative deviation between the ozone vertical distribution of OMPS and the ozone sonde data is less than 10% in the middle and upper stratosphere, but larger (15%-40%) in the middle and upper troposphere.
	Wang et al <sup>[114]</sup> used DOAS and multiplicative algebraic reconstruction to extract vertical ozone profiles from atmospheric limb scattering measurements. Comparing the extracted ozone profile with the ozone measurement of SCIAMACHY, the deviation of the two data is less than $\pm 10\%$ . Van Peet et al <sup>[115]</sup> improved the ozone profile retrieval algorithm (OPERA) and applied it to GOME and GOME-2 satellites. The ozone retrieval results of the two satellites are analyzed and verified with the data of the ultraviolet radiation data center (WOUUDC). It is suggested that the relative difference in the troposphere is 20%, while it in the stratosphere is 15%.
	Zawada et al <sup>[116]</sup> developed a two-dimensional tomography algorithm based on OMPS-LP, and compared the dataset of the developed algorithm with the MLS observations. Within 20 minutes, the difference in the stratosphere is less than 5%. Ma <sup>[8]</sup> developed a global tropospheric ozone dataset with long time series for OMI/MLS and TOMS/SBV, which improved the consistency of original ozone data and ground-based data by 44.89%.

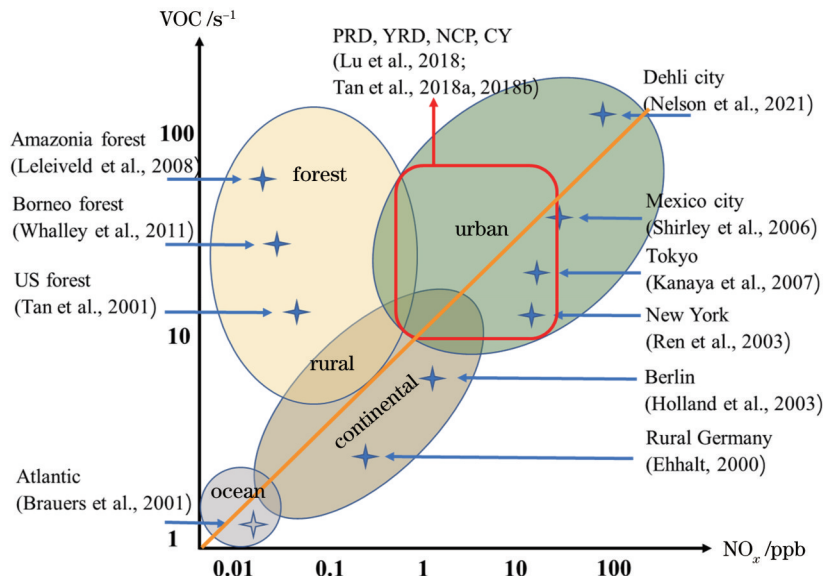
例如,Felipe-Sotelo等<sup>[118]</sup>收集了2000—2004年41个采样点的臭氧数据,确定了不同研究区的日均、周平均和年均臭氧分布,并在每个分区应用主成分分析揭示了臭氧与大气污染物以及气象变量之间的关系。Xue等<sup>[119]</sup>融合现场观测、卫星遥感测量和空气质量模型模拟数据构建臭氧数据集,分析了2013—2017年中国臭氧的时空变化,发现人口加权臭氧平均值从2013年的86  $\mu\text{g}/\text{m}^3$ 增长到2017年的95  $\mu\text{g}/\text{m}^3$ 。

#### 4.2.2 典型污染事件分析

典型臭氧污染过程分析可以更加清晰地阐明近地面臭氧污染的生成机理、发展过程和后续演变规律。根据大气化学反应机理,臭氧的形成实际上是VOC<sub>s</sub>和NO<sub>x</sub>争夺自由基的过程。[图5](#)总结了典型地区的VOC<sub>s</sub>与NO<sub>x</sub>控制区分析情况,脊线表示臭氧等值线拐点的连接线。脊线上方处于NO<sub>x</sub>控制区,VOC<sub>s</sub>/NO<sub>x</sub>

较大,臭氧浓度多受NO<sub>x</sub>变化的影响;脊线下方处于VOC<sub>s</sub>控制区,VOC<sub>s</sub>/NO<sub>x</sub>较小,臭氧浓度多受VOC<sub>s</sub>变化的影响,且臭氧浓度会随着NO<sub>x</sub>浓度增加而降低。

在海洋地区,Brauers等<sup>[120]</sup>收集了5°N和40°S之间的483个OH浓度数据,分析了热带大西洋中OH自由基参与对流层臭氧的化学过程。此外,Tan等<sup>[121]</sup>、Lelieveld等<sup>[122]</sup>和Whalley等<sup>[123]</sup>分别在美国的密歇根州北部森林、亚马孙森林、婆罗洲雨林等森林地区分析了OH的变化情况,进一步阐明了VOC<sub>s</sub>和NO<sub>x</sub>争夺自由基的化学机制。Ehhalt等<sup>[124]</sup>实地调查了德国东北部相对未受污染的农村地区的OH浓度,发现OH对NO<sub>x</sub>的高度非线性依赖性可以用Padé函数近似。同时,他们开发了一种OH对UV和二氧化氮的依赖性定量化的分析方法,该方法可消除由变量UV和二氧化氮依赖性而引起的OH变化。除了上述典型地区

图5 典型地区的VOC<sub>s</sub>与NO<sub>x</sub>控制区分析(图中斜线为“脊线”)Fig. 5 Analysis of VOC<sub>s</sub> and NO<sub>x</sub> control zones in typical areas (Diagonal line in figure is 'ridge line')

外,城镇地区的污染事件分析在总体研究中占很大的比例,且不同地区臭氧污染产生的原理和性质都各不相同。Shirley等<sup>[125]</sup>测量了2003年4月墨西哥的OH和HO<sub>2</sub>浓度,发现在化学反应过程中HO<sub>2</sub>/OH与NO的依赖性基本相同,但在NO接近于100 ppbv(按体积计算的十亿分之一)时除外。Kanaya等<sup>[126]</sup>在东京测量了OH和HO<sub>2</sub>的浓度,发现白天的HO<sub>2</sub>浓度在冬季被低估,特别是在冬季的早上,而在夏季却被高估。Nelson等<sup>[127]</sup>在印度德里测量了特定非甲烷烃挥发性有机化合物(C2-C13)、氧化挥发性有机化合物、NO、NO<sub>2</sub>、HONO、CO、SO<sub>2</sub>、臭氧和光解速率的浓度,调试了VOC<sub>s</sub>与NO<sub>x</sub>在模型中的变化,发现仅降低NO<sub>x</sub>浓度时,臭氧浓度显著增加;且仅减少道路运输排放量时,臭氧浓度显著增加。这些发现强调了在当地污染减排过程中,NO<sub>x</sub>、颗粒物与VOCs协同减少的重要性。在我国,Tan等<sup>[128-129]</sup>和Lu等<sup>[130]</sup>阐述了在京津冀、长三角、珠三角和成渝地区EKMA曲线中VOC<sub>s</sub>和NO<sub>x</sub>争夺自由基的情况,发现城区易出现臭氧高污染;而处于高臭氧污染城区下风向的市郊和乡村地区,受城区光化学烟雾前体物排放的影响也会出现严重的臭氧污染。

总之,对臭氧典型污染事件的成因进行分析具有重要意义,可以帮助人们理清臭氧典型污染事件的形成源头,从而更为科学地开展管控和治理。卫星遥感反演的近地面臭氧浓度数据集为这些研究提供了最为关键的数据支撑。

#### 4.2.3 臭氧污染与气象条件相互作用

气象条件是影响近地面臭氧生成的关键要素,而不同地区的气象条件各不相同。因此,研究臭氧污染与气象条件间的相互作用同样具有很大难度,并具有

重要科学意义和实际价值。

以往研究表明,降水、气温、相对湿度、日照时间、地面气压和风速是影响地面臭氧浓度的主要因素<sup>[131]</sup>。通过分离气象条件和人为排放的影响,Yin等<sup>[132]</sup>发现臭氧主导模态的变化由气象条件变化而引起,同时也验证了位于中国东部上方的异常反气旋环流会产生干热空气和更强的光化学反应,并将臭氧输送到地表。作为北半球主要的遥相关模态,亚欧大陆模态的正相位可以调节当地的气象条件,增强光化学反应,从而增加北半球的臭氧浓度<sup>[133]</sup>。东亚夏季风也显著影响了中国近地面臭氧污染的年际变化<sup>[134]</sup>。在日时间尺度上,由于高温可以促进光化学反应,相对湿度较低的区域会出现严重的臭氧污染<sup>[135-138]</sup>,较高的相对湿度通常与较大的大气不稳定性和云量有关,它会导致光化学反应减缓,近地面臭氧浓度降低<sup>[139-140]</sup>。此外,相对湿度的增加更容易产生降水清除、光化学反应效率降低、氧原子减少和羟基自由基增加,进而降低臭氧浓度<sup>[102,141-142]</sup>。因此,湿度较高、云层较多、太阳辐射较少和气温较低等环境条件不利于臭氧形成<sup>[143-144]</sup>。

臭氧污染的发生是其前体物排放在多种不同气象要素影响下的共同作用结果,而卫星遥感反演的近地面臭氧浓度数据集提供了研究臭氧污染与气象条件相互作用的数据基础。

#### 4.3 平流层臭氧区域传输和辐射效应

在特定的天气系统下,平流层臭氧可经过平流层-对流层交换(STE)侵入对流层,有时会导致地面臭氧急剧增加<sup>[145-148]</sup>。STE过程多发生在春、冬季,且在确定对流层臭氧收支中起重要作用,占北半球中纬度地区臭氧资源的20%~30%<sup>[7]</sup>。此外,STE的出现多与气旋、锋面、Brewer-Dobson环流、对流层顶折迭、

Rossby破碎和湿对流等动力过程相关<sup>[149-153]</sup>。遥感卫星通过识别水蒸气通道(6.2、6.5、6.9 μm)中水分含量来确定对流层顶和平流层底的动态条件,美国NOAA全球预报系统模型采用此方法,可识别部分平流层侵入事件<sup>[154]</sup>。

Knowland等<sup>[146]</sup>结合观测数据、MERRA-2再分析和Goddard地球观测系统模型,分析和验证了科罗拉多州2012年春季平流层侵入造成臭氧严重超标事件。Lin等<sup>[148]</sup>采用全球高分辨率全球化学-气候模型(GFDL AM3),结合地面测量结果、激光雷达数据和臭氧柱总量浓度,发现平流层侵入对美国西部高海拔地区春季臭氧污染事件起重要作用。Langford等<sup>[154]</sup>选用两个时间段(2013-05-19—2013-06-04和2013-06-22—2013-06-28)的OMI臭氧柱总量(地表至~2.5 km)、激光雷达的后向散射廓线、地基臭氧观测和气象参数等数据,分析了内华达州克拉克县三次臭氧超标的成因,发现来自亚洲的长距离运输对地面臭氧的贡献较小(<10 ppbv)。刘宁微<sup>[155]</sup>选用2010—2012年期间中国区域的6个大气观测站数据,结合高分辨全球大气化学-环流模式(EMAC)、OMI臭氧柱总量和MLS臭氧廓线数据,调查了中国地区的对流层臭氧时空分布特征,研究了不同大陆污染源远距离输送对中国不同地区臭氧变化的影响。Gao等<sup>[156]</sup>利用GEOS-Chem模型描述了生物质燃烧排放对美国西部地表臭氧的潜在影响,并将结果与CASTNet地表臭氧观测数据进行对比分析,发现两种地面臭氧资料具有较好的一致性,且近地面臭氧浓度与生物质燃示踪剂的变化密切相关。Tarasick等<sup>[157]</sup>利用高分辨风廓线雷达测量对流层顶的快速变化来追踪平流层入侵,研究发现,春夏季平流层-对流层交换(STT)事件约2~3天发生一次,而秋冬季STT事件频率降到4~5天/次。将0~1 km、1~3 km和3~8 km分别定义为边界层、对流层底层和对流层中高层,分析七次STT运动发现,边界层臭氧(1.2 ppb)平均占3.1%,但对流层低层臭氧(5.4 ppb)平均占13%,对流层中高层(22 ppb)平均占34%。此外,臭氧STT过程还会对海洋热量吸收产生影响。Liu等<sup>[158]</sup>通过分析1955—2000年间臭氧变化对南大洋2 km上层海洋净热量的影响,发现海洋净热量增加约30%,其中约60%的增加归因于对流层,40%归因于平流层损耗,这说明平流层和对流层的臭氧变化都对南大洋内部变暖作出了贡献,对流层臭氧的贡献更大一些。同时,他们还分析了两种增暖效应的物理机制:对流层臭氧增加主要通过等密度线的加深引起南大洋次表层变暖,而平流层臭氧损耗则通过沿500 m上层等密度线的细微变化来增暖。

此外,高空臭氧可吸收大量来自太阳的紫外辐射,在为地球生命体提供保护功能的同时加热高层大气,改变高层大气稳定性。Xia等<sup>[159]</sup>基于多传感器再分析版本2(MSR-2)臭氧数据、ERA5再分析资料中的月平

均温度、水汽和云分数等数据系统地揭示了2020年西伯利亚北极臭氧的减少导致该地区异常变暖,发现2020年4月和5月西伯利亚北极的最大陆地表面温度升高分别达8.8 K和6.2 K。其主要机制是2020年创纪录的北极臭氧消耗在4月和5月转移到西伯利亚中部,导致平流层下部局部变冷,进而导致对流层高层大气稳定度的降低,使得高云增加,从而通过正的长波云辐射强迫效应促进西伯利亚北极的地表变暖。在此基础上,Xia等<sup>[160]</sup>发现臭氧损耗通过增加高云可能导致西伯利亚北极地区春季地表紫外辐射减少而非增加。Wang等<sup>[161]</sup>采用MLS臭氧数据、MERRA2数据、ERA5再分析资料和观测数据分析了STT臭氧辐射通量,研究表明,ERA5、MERRA2和观测资料中温带下行的臭氧通量分别为538 Tg year<sup>-1</sup>、543 Tg year<sup>-1</sup>和528~539 Tg year<sup>-1</sup>,考虑热带上行的臭氧通量后,ERA5、MERRA2和观测资料中全球臭氧STE的通量分别为346 Tg year<sup>-1</sup>、360 Tg year<sup>-1</sup>和336~346 Tg year<sup>-1</sup>,这些估算值显示热带上行的臭氧通量可补偿约35%的下行臭氧通量,进一步说明热带上行臭氧通量对于估计全球臭氧STE至关重要。同时,研究还发现云层辐射效应使全球臭氧STE增加了约21%~29%。

## 5 结 论

国际上陆续发射了高光谱观测卫星、大气环境监测卫星等多种卫星载荷,在空间分辨率、信噪比和垂直结构等多方面得到提升,已经可以满足多性能的臭氧反演。臭氧卫星遥感算法分类众多,目前臭氧柱总量监测精度较高,但与人类活动密切相关的近地面臭氧浓度的反演精度还有待提高。臭氧污染的大气化学过程较为复杂,其中臭氧主要前体物 NO<sub>x</sub> 和 VOC<sub>s</sub> 的遥感监测和争夺自由基的过程、近地面臭氧污染的区域传输和平流层臭氧侵入的识别分析过程、臭氧和PM<sub>2.5</sub> 大气复合污染解析过程等均是目前臭氧研究的重点。臭氧污染的监管和防控需要摸清来源,准确评估污染的成因,可从前体物排放、化学转化、气象影响、三维传输等方面逐步进行解析。并且不同的区域特征各不相同,关键是要控制臭氧的前体物排放,特别是VOC<sub>s</sub> 和 NO<sub>x</sub>。但 VOC<sub>s</sub> 种类繁多,目前只针对 HCHO 和 CHOCHO 开展了少量的卫星遥感监测,其反演精度、产品应用、地面观测和机载观测验证均是未来大气污染的重要研究内容。我国大气污染是大气复合型污染,臭氧和PM<sub>2.5</sub> 是大气复合污染的两个关键污染物,臭氧的治理需要 VOC<sub>s</sub> 和 NO<sub>x</sub> 的协同减排、精细化管控才有可能实现短期治标与长期治本之间的统一。

## 参 考 文 献

- [1] Das S S, Ratnam M V, Uma K N, et al. Influence of tropical cyclones on tropospheric ozone: possible implications[J]. Atmospheric Chemistry and Physics, 2016, 16(8): 4837-4847.
- [2] Mohanakumar K. Stratosphere troposphere interactions: an

- introduction[M]. New York: Springer, 2008.
- [3] Lu X, Hong J Y, Zhang L, et al. Severe surface ozone pollution in China: a global perspective[J]. *Environmental Science & Technology Letters*, 2018, 5(8): 487-494.
- [4] McKenzie R L, Aucamp P J, Bais A F, et al. Ozone depletion and climate change: impacts on UV radiation[J]. *Photochemical & Photobiological Sciences*, 2011, 10(2): 182-198.
- [5] Zhang J J, Wei Y J, Fang Z F. Ozone pollution: a major health hazard worldwide[J]. *Frontiers in Immunology*, 2019, 10: 2518.
- [6] 钟芳.香港地区臭氧时空变化特征及成因分析[D].南京:南京大学, 2015: 6-9.  
Zhong F. Study of spatial and temporal variations of ozone and its main causes in Hong Kong[D]. Nanjing: Nanjing University, 2015: 6-9.
- [7] Lelieveld J, Dentener F J. What controls tropospheric ozone?[J]. *Journal of Geophysical Research: Atmospheres*, 2000, 105(D3): 3531-3551.
- [8] 马明亮.对流层臭氧时空分析影响因素研究及近地面臭氧估算[J].测绘学报, 2020, 49(11): 1507.  
Ma M L. Study on influencing factors of temporal and spatial analysis of tropospheric ozone and estimation of near-surface ozone[J]. *Acta Geodaetica et Cartographica Sinica*, 2020, 49(11): 1507.
- [9] Ancellet G, Daskalakis N, Raut J C, et al. Analysis of the latitudinal variability of tropospheric ozone in the arctic using the large number of aircraft and ozonesonde observations in early summer 2008[J]. *Atmospheric Chemistry and Physics*, 2016, 16(20): 13341-13358.
- [10] Oikonomakis E, Aksoyoglu S, Wild M, et al. Solar "brightening" impact on summer surface ozone between 1990 and 2010 in Europe - a model sensitivity study of the influence of the aerosol - radiation interactions[J]. *Atmospheric Chemistry and Physics*, 2018, 18(13): 9741-9765.
- [11] David L M, Girach I A, Nair P R. Distribution of ozone and its precursors over Bay of Bengal during winter 2009: role of meteorology[J]. *Annales Geophysicae*, 2011, 29(9): 1613-1627.
- [12] Döll P. Vulnerability to the impact of climate change on renewable groundwater resources: a global-scale assessment[J]. *Environmental Research Letters*, 2009, 4(3): 035006.
- [13] Zhang W, Zou Y, Zheng X D, et al. Characteristics of the vertical distribution of tropospheric ozone in late autumn at Yangjiang Station in Pearl River Delta (PRD), China. Part I : observed event[J]. *Atmospheric Environment*, 2021, 244: 117898.
- [14] Pearce W, Holmberg K, Hellsten I, et al. Climate change on twitter: topics, communities and conversations about the 2013 IPCC working group 1 report[J]. *PLoS One*, 2014, 9(4): e94785.
- [15] Rider C F, Carlsten C. Air pollution and DNA methylation: effects of exposure in humans[J]. *Clinical Epigenetics*, 2019, 11(1): 1-15.
- [16] Baasandorj M, Fleming E L, Jackman C H, et al. O(<sup>1</sup>D) kinetic study of key ozone depleting substances and greenhouse gases[J]. *The Journal of Physical Chemistry A*, 2013, 117(12): 2434-2445.
- [17] 薛丽坤.中国地区低对流层高层大气化学与长距离输送特征研究[D].济南:山东大学, 2011: 63-112.  
Xue L K. Study on atmospheric chemistry and long-range transport at high altitudes in the lower troposphere over China [D]. Jinan: Shandong University, 2011: 63-112.
- [18] Cristofanelli P, Bracci A, Sprenger M, et al. Tropospheric ozone variations at the Nepal Climate Observatory-Pyramid (Himalayas, 5079 m a.s.l.) and influence of deep stratospheric intrusion events[J]. *Atmospheric Chemistry and Physics*, 2010, 10(14): 6537-6549.
- [19] Derwent R G, Utembe S R, Jenkin M E, et al. Tropospheric ozone production regions and the intercontinental origins of surface ozone over Europe[J]. *Atmospheric Environment*, 2015, 112: 216-224.
- [20] Safieddine S, Boynard A, Hao N, et al. Tropospheric ozone variability during the East Asian summer monsoon as observed by satellite (IASI), aircraft (MOZAIC) and ground stations[J]. *Atmospheric Chemistry and Physics*, 2016, 16(16): 10489-10500.
- [21] Liu H, Liu S, Xue B R, et al. Ground-level ozone pollution and its health impacts in China[J]. *Atmospheric Environment*, 2018, 173: 223-230.
- [22] Ponka A, Virtanen M. Chronic bronchitis, emphysema, and low -level air pollution in Helsinki, 1987-1989[J]. *Environmental Research*, 1994, 65(2): 207-217.
- [23] Lee D S, Holland M R, Falla N. The potential impact of ozone on materials in the U.K[J]. *Atmospheric Environment*, 1996, 30(7): 1053-1065.
- [24] Fishman J, Crutzen P J. The origin of ozone in the troposphere [J]. *Nature*, 1978, 274(5674): 855-858.
- [25] Seinfeld J H. Air pollution: a half century of progress[J]. *AIChE Journal*, 2004, 50(6): 1096-1108.
- [26] Walcek C J, Yuan H H. Calculated influence of temperature-related factors on ozone formation rates in the lower troposphere [J]. *Journal of Applied Meteorology*, 1995, 34(5): 1056-1069.
- [27] Dueñas C, Fernández M C, Canete S, et al. Assessment of ozone variations and meteorological effects in an urban area in the Mediterranean Coast[J]. *Science of the Total Environment*, 2002, 299(1/2/3): 97-113.
- [28] 陈世俭, 童俊超, Kobayashi Kazuhiko, 等.气象因子对近地面层臭氧浓度的影响[J].华中师范大学学报(自然科学版), 2005, 39(2): 273-277.  
Chen S J, Tong J C, Kobayashi K, et al. Influences of the meteorological factors on the ozone concentration near the ground [J]. *Journal of Central China Normal University (Natural Sciences)*, 2005, 39(2): 273-277.
- [29] Cooper O R, Parrish D D, Ziemke J, et al. Global distribution and trends of tropospheric ozone: an observation-based review [J]. *Elementa: Science of the Anthropocene*, 2014, 2: 29.
- [30] Trainer M, Parrish D D, Goldan P D, et al. Review of observation-based analysis of the regional factors influencing ozone concentrations[J]. *Atmospheric Environment*, 2000, 34(12/13/14): 2045-2061.
- [31] Lu X A, Zhang L, Wang X L, et al. Rapid increases in warm-season surface ozone and resulting health impact in China since 2013[J]. *Environmental Science & Technology Letters*, 2020, 7(4): 240-247.
- [32] Zhao Y B, Zhang K, Xu X T, et al. Substantial changes in nitrogen dioxide and ozone after excluding meteorological impacts during the COVID-19 outbreak in mainland China[J]. *Environmental Science & Technology Letters*, 2020, 7(6): 402-408.
- [33] Li T W, Cheng X. Estimating daily full-coverage surface ozone concentration using satellite observations and a spatiotemporally embedded deep learning approach[J]. *International Journal of Applied Earth Observation and Geoinformation*, 2021, 101: 102356.
- [34] Dave J V, Mateer C L. A preliminary study on the possibility of estimating total atmospheric ozone from satellite measurements [J]. *Journal of the Atmospheric Sciences*, 1967, 24(4): 414-427.
- [35] Petropavlovskikh I, Bhartia P K, DeLuisi J. New Umkehr ozone profile retrieval algorithm optimized for climatological studies[J]. *Geophysical Research Letters*, 2005, 32(16): L16808.
- [36] Coldewey-Egbers M, Weber M, Buchwitz M, et al. Application of a modified DOAS method for total ozone retrieval from GOME data at high polar latitudes[J]. *Advances in Space Research*, 2004, 34(4): 749-753.
- [37] Zhao F, Liu C, Cai Z N, et al. Ozone profile retrievals from TROPOMI: implication for the variation of tropospheric ozone

- during the outbreak of COVID-19 in China[J]. *Science of the Total Environment*, 2021, 764: 142886.
- [38] Calfapietra C, Fares S, Manes F, et al. Role of Biogenic Volatile Organic Compounds (BVOC) emitted by urban trees on ozone concentration in cities: a review[J]. *Environmental Pollution*, 2013, 183: 71-80.
- [39] Chang H H, Zhou J W, Fuentes M. Impact of climate change on ambient ozone level and mortality in southeastern United States[J]. *International Journal of Environmental Research and Public Health*, 2010, 7(7): 2866-2880.
- [40] Zhang Y Z, Wang Y H. Climate-driven ground-level ozone extreme in the fall over the Southeast United States[J]. *Proceedings of the National Academy of Sciences of the United States of America*, 2016, 113(36): 10025-10030.
- [41] 赵少华, 杨晓钰, 李正强, 等. 臭氧卫星遥感六十年进展[J]. 遥感学报, 2022, 26(5): 817-833.  
Zhao S H, Yang X Y, Li Z Q, et al. Advances of ozone satellite remote sensing in 60 years[J]. *National Remote Sensing Bulletin*, 2022, 26(5): 817-833.
- [42] Fan H, Zhao C F, Yang Y K. A comprehensive analysis of the spatio-temporal variation of urban air pollution in China during 2014-2018[J]. *Atmospheric Environment*, 2020, 220: 117066.
- [43] Ma Z Q, Xu J, Quan W J, et al. Significant increase of surface ozone at a rural site, north of Eastern China[J]. *Atmospheric Chemistry and Physics*, 2016, 16(6): 3969-3977.
- [44] Wang Q Y, Gao R S, Cao J J, et al. Observations of high level of ozone at Qinghai Lake Basin in the northeastern Qinghai-Tibetan Plateau, Western China[J]. *Journal of Atmospheric Chemistry*, 2015, 72(1): 19-26.
- [45] Ran L, Lin W L, Deji Y Z, et al. Surface gas pollutants in Lhasa, a highland city of Tibet-current levels and pollution implications[J]. *Atmospheric Chemistry and Physics*, 2014, 14 (19): 10721-10730.
- [46] Fujita E M, Campbell D E, Stockwell W R, et al. Past and future ozone trends in California's South Coast Air Basin: reconciliation of ambient measurements with past and projected emission inventories[J]. *Journal of the Air & Waste Management Association*, 2013, 63(1): 54-69.
- [47] Ou J M, Yuan Z B, Zheng J Y, et al. Ambient ozone control in a photochemically active region: short-term despiking or long-term attainment? [J]. *Environmental Science & Technology*, 2016, 50(11): 5720-5728.
- [48] Theys N, van Roozendael M, Hendrick F, et al. Global observations of tropospheric BrO columns using GOME-2 satellite data[J]. *Atmospheric Chemistry and Physics*, 2011, 11 (4): 1791-1811.
- [49] Ebojie F, von Savigny C, Ladstätter-Weißenmayer A, et al. Tropospheric column amount of ozone retrieved from SCIAMACHY limb-nadir-matching observations[J]. *Atmospheric Measurement Techniques*, 2014, 7(7): 2073-2096.
- [50] Eskes H J, Brinksma E J, Veefkind J P, et al. Retrieval and validation of ozone columns derived from measurements of SCIAMACHY on Envisat[J]. *Atmospheric Chemistry and Physics Discussions*, 2005, 5(4): 4429-4475.
- [51] Zhang C X, Liu C, Hu Q H, et al. Satellite UV-Vis spectroscopy: implications for air quality trends and their driving forces in China during 2005-2017[J]. *Light: Science & Applications*, 2019, 8: 100.
- [52] Flynn L E, Homstein J, Hilsenrath E. The ozone mapping and profiler suite (OMPS). The next generation of US ozone monitoring instruments[C]//2004 IEEE International Geoscience and Remote Sensing SymposiumI (GARSS), September 20-24, Anchorage, AK, USA. New York: IEEE Press, 2004: 1-4.
- [53] Flynn L, Long C, Wu X, et al. Performance of the ozone mapping and profiler suite (OMPS) products[J]. *Journal of Geophysical Research: Atmospheres*, 2014, 119(10): 6181-6195.
- [54] Garane K, Koukouli M E, Verhoelst T, et al. TROPOMI/S5P total ozone column data: global ground-based validation and consistency with other satellite missions[J]. *Atmospheric Measurement Techniques*, 2019, 12(10): 5263-5287.
- [55] Mettig N, Weber M, Rozanov A, et al. Combined UV and IR ozone profile retrieval from TROPOMI and CrIS measurements [J]. *Atmospheric Measurement Techniques*, 2022, 15(9): 2955-2978.
- [56] Zhang C X, Liu C, Wang Y, et al. Preflight evaluation of the performance of the Chinese environmental trace gas monitoring instrument (EMI) by spectral analyses of nitrogen dioxide[J]. *IEEE Transactions on Geoscience and Remote Sensing*, 2018, 56(6): 3323-3332.
- [57] Zhang C X, Liu C, Chan K L, et al. First observation of tropospheric nitrogen dioxide from the Environmental Trace Gases Monitoring Instrument onboard the GaoFen-5 satellite[J]. *Light: Science & Applications*, 2020, 9: 66.
- [58] Xia C Z, Liu C, Cai Z N, et al. First sulfur dioxide observations from the environmental trace gases monitoring instrument (EMI) onboard the GeoFen-5 satellite[J]. *Science Bulletin*, 2021, 66 (10): 969-973.
- [59] Coheur P F, Barret B, Turquety S, et al. Retrieval and characterization of ozone vertical profiles from a thermal infrared nadir sounder[J]. *Journal of Geophysical Research: Atmospheres*, 2005, 110(D24): D24303.
- [60] Divakarla M, Barnet C, Goldberg M, et al. Evaluation of Atmospheric Infrared Sounder ozone profiles and total ozone retrievals with matched ozonesonde measurements, ECMWF ozone data, and Ozone Monitoring Instrument retrievals[J]. *Journal of Geophysical Research: Atmospheres*, 2008, 113 (D15): D15308.
- [61] Nassar R, Logan J A, Worden H M, et al. Validation of Tropospheric Emission Spectrometer (TES) nadir ozone profiles using ozonesonde measurements[J]. *Journal of Geophysical Research: Atmospheres*, 2008, 113(D15): D15S17.
- [62] Clerbaux C, Boynard A, Clarisse L, et al. Monitoring of atmospheric composition using the thermal infrared IASI/MetOp sounder[J]. *Atmospheric Chemistry and Physics*, 2009, 9(16): 6041-6054.
- [63] Boynard A, Clerbaux C, Coheur P F, et al. Measurements of total and tropospheric ozone from IASI: comparison with correlative satellite, ground-based and ozonesonde observations [J]. *Atmospheric Chemistry and Physics*, 2009, 9(16): 6255-6271.
- [64] Ma P F, Chen L F, Wang Z T, et al. Ozone profile retrievals from the cross-track infrared sounder[J]. *IEEE Transactions on Geoscience and Remote Sensing*, 2016, 54(7): 3985-3994.
- [65] 王雅鹏, 李小英, 陈良富, 等. 红外临边探测发展现状[J]. 遥感学报, 2016, 20(4): 513-527.  
Wang Y P, Li X Y, Chen L F, et al. Overview of infrared limb sounding[J]. *Journal of Remote Sensing*, 2016, 20(4): 513-527.
- [66] Wellemeyer C G, Bhartia P K, McPeters R D, et al. A new release of data from the Total Ozone Mapping Spectrometer (TOMS)[J]. *SPARC Newsletter*, 2004, 22: 37-38.
- [67] Balis D, Kroon M, Koukouli M E, et al. Validation of Ozone Monitoring Instrument total ozone column measurements using Brewer and Dobson spectrophotometer ground-based observations[J]. *Journal of Geophysical Research: Atmospheres*, 2007, 112(D24): D24S46.
- [68] 张莹, 高场, 祝善友, 等. 近30a中国上空臭氧总量时空变化遥感监测分析[J]. 地球信息科学学报, 2014, 16(6): 971-978.  
Zhang Y, Gao Y, Zhu S Y, et al. Variation of total ozone over China for 30 years analyzed by multi-source satellite remote sensing data[J]. *Journal of Geo-Information Science*, 2014, 16 (6): 971-978.
- [69] 张艳, 王维和, 张兴羸. 卫星遥感监测大气臭氧总量分布和变化[J]. 科技导报, 2015, 33(17): 23-29.

- Zhang Y, Wang W H, Zhang X Y. Distribution and variation of atmospheric total column ozone based on satellite remote sensing data[J]. *Science & Technology Review*, 2015, 33(17): 23-29.
- [70] 彭晓琳. 全球卫星臭氧产品的时空重建研究[D]. 武汉: 武汉大学, 2017.
- Peng X L. Spatio-temporal reconstruction for globally remotely sensed total ozone production[D]. Wuhan: Wuhan University, 2017.
- [71] Rodgers C D. Retrieval of atmospheric temperature and composition from remote measurements of thermal radiation[J]. *Reviews of Geophysics*, 1976, 14(4): 609-624.
- [72] Bhartia P K, McPeters R D, Flynn L E, et al. Solar Backscatter UV (SBUV) total ozone and profile algorithm[J]. *Atmospheric Measurement Techniques*, 2013, 6(10): 2533-2548.
- [73] Ziemke J R, Chandra S, Duncan B N, et al. Tropospheric ozone determined from Aura OMI and MLS: Evaluation of measurements and comparison with the Global Modeling Initiative's Chemical Transport Model[J]. *Journal of Geophysical Research: Atmospheres*, 2006, 111(D19): D19303.
- [74] Huang F X, Liu N Q, Zhao M X, et al. Vertical ozone profiles deduced from measurements of SBUS on FY-3 satellite[J]. *Chinese Science Bulletin*, 2010, 55(10): 943-948.
- [75] 黄富祥, 赵明现, 杨昌军, 等. 风云三号卫星紫外臭氧垂直廓线反演算法及对比反演试验[J]. 自然科学进展, 2008, 18(10): 1136-1142.
- Huang F X, Zhao M X, Yang C J, et al. Inversion algorithm and comparative inversion test of vertical profile of ultraviolet ozone in Fengyun-3 satellite[J]. *Progress in Natural Science*, 2008, 18(10): 1136-1142.
- [76] Miles G M, Siddans R, Kerridge B J, et al. Tropospheric ozone and ozone profiles retrieved from GOME-2 and their validation [J]. *Atmospheric Measurement Techniques*, 2015, 8(1): 385-398.
- [77] Flynn L, Long C, Wu X, et al. Performance of the ozone mapping and profiler suite (OMPS) products[J]. *Journal of Geophysical Research: Atmospheres*, 2014, 119(10): 6181-6195.
- [78] Arosio C, Rozanov A, Malinina E, et al. Retrieval of ozone profiles from OMPS limb scattering observations[J]. *Atmospheric Measurement Techniques*, 2018, 11(4): 2135-2149.
- [79] 刘诚. 一种卫星遥感大气臭氧廓线反演算法: CN108760662A[P]. 2018-11-06.
- Liu C. Satellite remote sensing atmospheric ozone profile inversion algorithm: CN108760662A[P]. 2018-11-06.
- [80] Kroon M, de Haan J F, Veefkind J P, et al. Validation of operational ozone profiles from the Ozone Monitoring Instrument [J]. *Journal of Geophysical Research: Atmospheres*, 2011, 116 (D18): D18305.
- [81] Bak J, Liu X, Wei J C, et al. Improvement of OMI ozone profile retrievals in the upper troposphere and lower stratosphere by the use of a tropopause-based ozone profile climatology[J]. *Atmospheric Measurement Techniques*, 2013, 6(9): 2239-2254.
- [82] Susskind J, Barnet C D, Blaisdell J M. Retrieval of atmospheric and surface parameters from AIRS/AMSU/HSB data in the presence of clouds[J]. *IEEE Transactions on Geoscience and Remote Sensing*, 2003, 41(2): 390-409.
- [83] Wei J C, Pan L L, Maddy E, et al. Ozone profile retrieval from an advanced infrared sounder: experiments with tropopause-based climatology and optimal estimation approach[J]. *Journal of Atmospheric and Oceanic Technology*, 2010, 27(7): 1123-1139.
- [84] Bowman K W, Rodgers C D, Kulawik S S, et al. Tropospheric emission spectrometer: retrieval method and error analysis[J]. *IEEE Transactions on Geoscience and Remote Sensing*, 2006, 44(5): 1297-1307.
- [85] Worden H M, Logan J A, Worden J R, et al. Comparisons of Tropospheric Emission Spectrometer (TES) ozone profiles to ozonesondes: methods and initial results[J]. *Journal of Geophysical Research: Atmospheres*, 2007, 112(D3): D03309.
- [86] Natraj V, Liu X, Kulawik S, et al. Multi-spectral sensitivity studies for the retrieval of tropospheric and lowermost tropospheric ozone from simulated clear-sky GEO-CAPE measurements[J]. *Atmospheric Environment*, 2011, 45(39): 7151-7165.
- [87] Zhang X X, Zhang Y, Lu X Y, et al. Estimation of lower-stratosphere-to-troposphere ozone profile using long short-term memory (LSTM)[J]. *Remote Sensing*, 2021, 13(7): 1374.
- [88] Fishman J, Larsen J C. Distribution of total ozone and stratospheric ozone in the tropics: implications for the distribution of tropospheric ozone[J]. *Journal of Geophysical Research: Atmospheres*, 1987, 92(D6): 6627-6634.
- [89] Kim J H, Hudson R D, Thompson A M. A new method of deriving time-averaged tropospheric column ozone over the tropics using total ozone mapping spectrometer (TOMS) radiances: Intercomparison and analysis using TRACE A data [J]. *Journal of Geophysical Research: Atmospheres*, 1996, 101 (D19): 24317-24330.
- [90] Hudson R D, Thompson A M. Tropical tropospheric ozone from total ozone mapping spectrometer by a modified residual method[J]. *Journal of Geophysical Research: Atmospheres*, 1998, 103(D17): 22129-22145.
- [91] Schoeberl M R, Ziemke J R, Bojkov B, et al. A trajectory-based estimate of the tropospheric ozone column using the residual method[J]. *Journal of Geophysical Research: Atmospheres*, 2007, 112(D24): D24S49.
- [92] Kim J H, Newchurch M J, Han K. Distribution of tropical tropospheric ozone determined by the scan-angle method applied to TOMS measurements[J]. *Journal of the Atmospheric Sciences*, 2001, 58(18): 2699-2708.
- [93] Ziemke J R, Chandra S, Bhartia P K. "Cloud slicing": a new technique to derive upper tropospheric ozone from satellite measurements[J]. *Journal of Geophysical Research: Atmospheres*, 2001, 106(D9): 9853-9867.
- [94] Cobourn W G, Dolcine L, French M, et al. A comparison of nonlinear regression and neural network models for ground-level ozone forecasting[J]. *Journal of the Air & Waste Management Association*, 2000, 50(11): 1999-2009.
- [95] Cannon A J, Lord E R. Forecasting summertime surface-level ozone concentrations in the lower Fraser valley of British Columbia: an ensemble neural network approach[J]. *Journal of the Air & Waste Management Association*, 2000, 50(3): 322-339.
- [96] Chaloulakou A, Saisana M, Spyrellis N. Comparative assessment of neural networks and regression models for forecasting summertime ozone in Athens[J]. *Science of the Total Environment*, 2003, 313(1/2/3): 1-13.
- [97] Wang W J, Lu W Z, Wang X K, et al. Prediction of maximum daily ozone level using combined neural network and statistical characteristics[J]. *Environment International*, 2003, 29(5): 555-562.
- [98] Chattopadhyay S, Bandyopadhyay G. Artificial neural network with backpropagation learning to predict mean monthly total ozone in Arosa, Switzerland[J]. *International Journal of Remote Sensing*, 2007, 28(20): 4471-4482.
- [99] 张海传, 刘钟阳, 许东卫, 等. 基于RBF神经网络模型的臭氧浓度软测量研究[J]. 大连理工大学学报, 2010, 50(6): 1020-1023.
- Zhang H C, Liu Z Y, Xu D W, et al. Research on software sensor of ozone concentration based on RBF neural networks model[J]. *Journal of Dalian University of Technology*, 2010, 50 (6): 1020-1023.
- [100] Luna A S, Paredes M L L, de Oliveira G C G, et al. Prediction of ozone concentration in tropospheric levels using artificial neural networks and support vector machine at Rio de Janeiro,

- Brazil[J]. Atmospheric Environment, 2014, 98: 98-104.
- [101] Taylan O. Modelling and analysis of ozone concentration by artificial intelligent techniques for estimating air quality[J]. Atmospheric Environment, 2017, 150: 356-365.
- [102] Gao M, Yin L T, Ning J C. Artificial neural network model for ozone concentration estimation and Monte Carlo analysis[J]. Atmospheric Environment, 2018, 184: 129-139.
- [103] Liu R Y, Ma Z W, Liu Y, et al. Spatiotemporal distributions of surface ozone levels in China from 2005 to 2017: a machine learning approach[J]. Environment International, 2020, 142: 105823.
- [104] Zhang X Y, Zhao L M, Cheng M M, et al. Estimating ground-level ozone concentrations in Eastern China using satellite-based precursors[J]. IEEE Transactions on Geoscience and Remote Sensing, 2020, 58(7): 4754-4763.
- [105] Li R, Zhao Y L, Zhou W H, et al. Developing a novel hybrid model for the estimation of surface 8 h ozone ( $O_3$ ) across the remote Tibetan Plateau during 2005 - 2018[J]. Atmospheric Chemistry and Physics, 2020, 20(10): 6159-6175.
- [106] DeLang M N, Becker J S, Chang K L, et al. Mapping yearly fine resolution global surface ozone through the Bayesian maximum entropy data fusion of observations and model output for 1990 - 2017[J]. Environmental Science & Technology, 2021, 55(8): 4389-4398.
- [107] Wang Y, Yuan Q Q, Zhu L Y, et al. Spatiotemporal estimation of hourly 2-km ground-level ozone over China based on Himawari-8 using a self-adaptive geospatially local model[J]. Geoscience Frontiers, 2022, 13(1): 101286.
- [108] Bian J C, Chen H B, Zhao Y L, et al. Variation features of total atmospheric ozone in Beijing and Kunming based on Dobson and TOMS data[J]. Advances in Atmospheric Sciences, 2002, 19 (2): 279-286.
- [109] 陈丹, 周斌, 陈立民. 利用天顶散射光观测反演大气臭氧柱浓度[J]. 复旦学报(自然科学版), 2008, 47(4): 478-486.
- Chen D, Zhou B, Chen L M. The retrieval of atmospheric ozone column densities using zenith-sky scattered light observations[J]. Journal of Fudan University (Natural Science), 2008, 47(4): 478-486.
- [110] Hong H, Lee H, Kim J, et al. First comparison of OMI-DOAS total ozone using ground-based observations at a megacity site in East Asia: causes of discrepancy and improvement in OMI-DOAS total ozone during summer[J]. Journal of Geophysical Research: Atmospheres, 2014, 119(16): 10058-10067.
- [111] 蔡兆男, 王永, 郑向东, 等. 利用探空资料验证GOME卫星臭氧数据[J]. 应用气象学报, 2009, 20(3): 337-345.
- Cai Z N, Wang Y, Zheng X D, et al. Validation of GOME ozone profiles and tropospheric column ozone with ozone sonde over China[J]. Journal of Applied Meteorological Science, 2009, 20(3): 337-345.
- [112] 张雷, 丁明虎, 卞林根, 等. AIRS卫星温度和臭氧廓线在南极的验证分析[J]. 地球物理学报, 2020, 63(4): 1318-1331.
- Zhang L, Ding M H, Bian L G, et al. Validation of AIRS temperature and ozone profiles over Antarctica[J]. Chinese Journal of Geophysics, 2020, 63(4): 1318-1331.
- [113] 陈源, 刘海磊, 段民征, 等. 利用探空资料验证北京地区OMPS卫星臭氧产品[J]. 遥感技术与应用, 2020, 35(3): 723-730.
- Chen Y, Liu H L, Duan M Z, et al. Validation of ozone product by satellite OMPS with sounding measurements over Beijing[J]. Remote Sensing Technology and Application, 2020, 35(3): 723-730.
- [114] Wang Z J, Chen S B, Yang C Y, et al. A method for retrieving vertical ozone profiles from limb scattered measurements[J]. Acta Meteorologica Sinica, 2011, 25(5): 659-668.
- [115] van Peet J C A, van der A R J, Tuinder O N E, et al. Ozone ProfilE Retrieval Algorithm (OPERA) for nadir-looking satellite instruments in the UV - VIS[J]. Atmospheric Measurement Techniques, 2014, 7(3): 859-876.
- [116] Zawada D J, Rieger L A, Bourassa A E, et al. Tomographic retrievals of ozone with the OMPS Limb Profiler: algorithm description and preliminary results[J]. Atmospheric Measurement Techniques, 2018, 11(4): 2375-2393.
- [117] Wu R R, Xie S D. Spatial distribution of ozone formation in China derived from emissions of speciated volatile organic compounds[J]. Environmental Science & Technology, 2017, 51 (5): 2574-2583.
- [118] Felipe-Sotelo M, Gustems L, Hernández I, et al. Investigation of geographical and temporal distribution of tropospheric ozone in Catalonia (North-East Spain) during the period 2000-2004 using multivariate data analysis methods[J]. Atmospheric Environment, 2006, 40(38): 7421-7436.
- [119] Xue T, Zheng Y X, Geng G N, et al. Estimating spatiotemporal variation in ambient ozone exposure during 2013 - 2017 using a data-fusion model[J]. Environmental Science & Technology, 2020, 54(23): 14877-14888.
- [120] Brauers T, Hausmann M, Bister A, et al. OH radicals in the boundary layer of the Atlantic Ocean: 1. Measurements by long-path laser absorption spectroscopy[J]. Journal of Geophysical Research: Atmospheres, 2001, 106(D7): 7399-7414.
- [121] Tan D, Faloona I, Simpas J B, et al. HO<sub>x</sub> budgets in a deciduous forest: results from the PROPHET summer 1998 campaign[J]. Journal of Geophysical Research: Atmospheres, 2001, 106(D20): 24407-24427.
- [122] Lelieveld J, Butler T M, Crowley J N, et al. Atmospheric oxidation capacity sustained by a tropical forest[J]. Nature, 2008, 452(7188): 737-740.
- [123] Whalley L K, Edwards P M, Furneaux K L, et al. Quantifying the magnitude of a missing hydroxyl radical source in a tropical rainforest[J]. Atmospheric Chemistry and Physics, 2011, 11 (14): 7223-7233.
- [124] Ehhalt D H, Rohrer F. Dependence of the OH concentration on solar UV[J]. Journal of Geophysical Research: Atmospheres, 2000, 105(D3): 3565-3571.
- [125] Shirley T R, Brune W H, Ren X, et al. Atmospheric oxidation in the Mexico city metropolitan area (MCMA) during April 2003 [J]. Atmospheric Chemistry and Physics, 2006, 6(9): 2753-2765.
- [126] Kanaya Y, Cao R Q, Akimoto H, et al. Urban photochemistry in central Tokyo: 1. Observed and modeled OH and HO<sub>2</sub> radical concentrations during the winter and summer of 2004[J]. Journal of Geophysical Research: Atmospheres, 2007, 112(D21): D21312.
- [127] Nelson B S, Stewart G J, Drysdale W S, et al. *In situ* ozone production is highly sensitive to volatile organic compounds in Delhi, India[J]. Atmospheric Chemistry and Physics, 2021, 21 (17): 13609-13630.
- [128] Tan Z F, Lu K D, Dong H B, et al. Explicit diagnosis of the local ozone production rate and the ozone-NO<sub>x</sub>-VOC sensitivities [J]. Science Bulletin, 2018, 63(16): 1067-1076.
- [129] Tan Z F, Lu K D, Jiang M, et al. Atmospheric oxidation capacity in Chinese megacities during photochemical polluted season: radical budget and secondary pollutants formation[J]. Atmospheric Chemistry and Physics, 2018: 1-23.
- [130] Lu K D, Guo S, Tan Z F, et al. Exploring atmospheric free-radical chemistry in China: the self-cleansing capacity and the formation of secondary air pollution[J]. National Science Review, 2019, 6(3): 579-594.
- [131] Tang G, Wang Y, Li X, et al. Spatial-temporal variations in surface ozone in Northern China as observed during 2009 - 2010 and possible implications for future air quality control strategies [J]. Atmospheric Chemistry and Physics, 2012, 12(5): 2757-2776.
- [132] Yin Z C, Ma X Q. Meteorological conditions contributed to changes in dominant patterns of summer ozone pollution in Eastern China[J]. Environmental Research Letters, 2020, 15

- (12): 124062.
- [133] Yin Z C, Wang H J, Li Y Y, et al. Links of climate variability in Arctic Sea ice, Eurasian teleconnection pattern and summer surface ozone pollution in North China[J]. *Atmospheric Chemistry and Physics*, 2019, 19(6): 3857-3871.
- [134] Yang Y, Liao H, Li J. Impacts of the East Asian summer monsoon on interannual variations of summertime surface-layer ozone concentrations over China[J]. *Atmospheric Chemistry and Physics*, 2014, 14(13): 6867-6879.
- [135] Pu X, Wang T J, Huang X, et al. Enhanced surface ozone during the heat wave of 2013 in Yangtze River Delta region, China[J]. *Science of the Total Environment*, 2017, 603/604: 807-816.
- [136] Otero N, Sillmann J, Schnell J L, et al. Synoptic and meteorological drivers of extreme ozone concentrations over Europe[J]. *Environmental Research Letters*, 2016, 11(2): 024005.
- [137] Li K, Jacob D J, Liao H, et al. Anthropogenic drivers of 2013-2017 trends in summer surface ozone in China[J]. *Proceedings of the National Academy of Sciences of the United States of America*, 2019, 116(2): 422-427.
- [138] 王敏, 方欣, 王毛翠, 等. 合肥地表臭氧变化特征及气象要素影响分析[J]. 大气与环境光学学报, 2022, 17(2): 205-212.
- Wang M, Fang X, Wang M C, et al. Analysis on variation characteristics of surface ozone and influence of meteorological elements in Hefei[J]. *Journal of Atmospheric and Environmental Optics*, 2022, 17(2): 205-212.
- [139] Camalier L, Cox W, Dolwick P. The effects of meteorology on ozone in urban areas and their use in assessing ozone trends[J]. *Atmospheric Environment*, 2007, 41(33): 7127-7137.
- [140] Chen Z Y, Li R Y, Chen D L, et al. Understanding the causal influence of major meteorological factors on ground ozone concentrations across China[J]. *Journal of Cleaner Production*, 2020, 242: 118498.
- [141] Jia L, Xu Y F. Effects of relative humidity on ozone and secondary organic aerosol formation from the photooxidation of benzene and ethylbenzene[J]. *Aerosol Science and Technology*, 2014, 48(1): 1-12.
- [142] Yu S C. Fog geoengineering to abate local ozone pollution at ground level by enhancing air moisture[J]. *Environmental Chemistry Letters*, 2019, 17(1): 565-580.
- [143] Zhao Z J, Wang Y X. Influence of the West Pacific subtropical high on surface ozone daily variability in summertime over Eastern China[J]. *Atmospheric Environment*, 2017, 170: 197-204.
- [144] 孙睿, 张红, 汪水兵, 等. 长三角区域典型城市臭氧时空分布及其与气象因素相关性研究[J]. 大气与环境光学学报, 2021, 16(6): 483-494.
- Sun R, Zhang H, Wang S B, et al. Temporal and spatial distribution of ozone in typical cities of Yangtze River Delta region and its correlation with meteorological factors[J]. *Journal of Atmospheric and Environmental Optics*, 2021, 16(6): 483-494.
- [145] Akritidis D, Zanis P, Pytharoulis I, et al. A deep stratospheric intrusion event down to the earth's surface of the megacity of Athens[J]. *Meteorology and Atmospheric Physics*, 2010, 109(1): 9-18.
- [146] Knowland K E, Ott L E, Duncan B N, et al. Stratospheric intrusion-influenced ozone air quality exceedances investigated in the NASA MERRA-2 reanalysis[J]. *Geophysical Research Letters*, 2017, 44(20): 10691-10701.
- [147] Lefohn A S, Wernli H, Shadwick D, et al. The importance of stratospheric-tropospheric transport in affecting surface ozone concentrations in the western and northern tier of the United States[J]. *Atmospheric Environment*, 2011, 45(28): 4845-4857.
- [148] Lin M Y, Fiore A M, Cooper O R, et al. Springtime high surface ozone events over the western United States: quantifying the role of stratospheric intrusions[J]. *Journal of Geophysical Research: Atmospheres*, 2012, 117(D21): D00V22.
- [149] Akritidis D, Katragkou E, Zanis P, et al. A deep stratosphere-to-troposphere ozone transport event over Europe simulated in CAMS global and regional forecast systems: analysis and evaluation[J]. *Atmospheric Chemistry and Physics*, 2018, 18(20): 15515-15534.
- [150] Holton J R, Haynes P H, McIntyre M E, et al. Stratosphere-troposphere exchange[J]. *Reviews of Geophysics*, 1995, 33(4): 403-439.
- [151] Krasauskas L, Ungermann J, Preusse P, et al. 3-D tomographic observations of Rossby wave breaking over the North Atlantic during the WISE aircraft campaign in 2017[J]. *Atmospheric Chemistry and Physics*, 2021, 21(13): 10249-10272.
- [152] Li D, Bian J C, Fan Q J. A deep stratospheric intrusion associated with an intense cut-off low event over East Asia[J]. *Science China Earth Sciences*, 2015, 58(1): 116-128.
- [153] Salby M L, Callaghan P F. Influence of the Brewer-Dobson circulation on stratosphere-troposphere exchange[J]. *Journal of Geophysical Research: Atmospheres*, 2006, 111(D21): D21106.
- [154] Langford A O, Senff C J, Alvarez R J, et al. An overview of the 2013 Las Vegas Ozone Study (LVOS): impact of stratospheric intrusions and long-range transport on surface air quality[J]. *Atmospheric Environment*, 2015, 109: 305-322.
- [155] 刘宁微. 中国区域近地面臭氧时空分布变化及远距离输送影响研究[D]. 北京: 中国气象科学研究院, 2019.
- Liu N W. Seasonal-spatial variations of surface ozone over China and the influence of long range transport[D]. Beijing: Chinese Academy of Meteorological Sciences, 2019.
- [156] Gao M, Li Q B, Mao Y H, et al. Biomass burning impact on surface ozone in the western United States[EB/OL]. [2023-02-05]. [https://projects.iq.harvard.edu/files/acmg-geos/files/icg5-day1-mon\\_posters\\_gao\\_mei\\_1\\_mac.pdf](https://projects.iq.harvard.edu/files/acmg-geos/files/icg5-day1-mon_posters_gao_mei_1_mac.pdf).
- [157] Tarasick D W, Carey-Smith T K, Hocking W K, et al. Quantifying stratosphere-troposphere transport of ozone using balloon-borne ozonesondes, radar wind profilers and trajectory models[J]. *Atmospheric Environment*, 2019, 198: 496-509.
- [158] Liu W, Hegglin M I, Checa-Garcia R, et al. Stratospheric ozone depletion and tropospheric ozone increases drive Southern Ocean interior warming[J]. *Nature Climate Change*, 2022, 12(4): 365-372.
- [159] Xia Y, Hu Y Y, Huang Y, et al. Significant contribution of severe ozone loss to the Siberian-Arctic surface warming in spring 2020[J]. *Geophysical Research Letters*, 2021, 48(8): e2021GL092509.
- [160] Xia Y, Wang Y W, Huang Y, et al. Significant contribution of stratospheric water vapor to the poleward expansion of the Hadley circulation in autumn under greenhouse warming[J]. *Geophysical Research Letters*, 2021, 48(17): e2021GL094008.
- [161] Wang M C, Fu Q. Stratosphere-troposphere exchange of air masses and ozone concentrations based on reanalyses and observations[J]. *Journal of Geophysical Research: Atmospheres*, 2021, 126(18): e2021JD035159.

# Progress and Challenges of Ozone Satellite Remote Sensing Inversion

Chi Yulei<sup>1</sup>, Zhao Chuanfeng<sup>2\*</sup>

<sup>1</sup>College of Global Change and Earth System Sciences, Beijing Normal University, Beijing 100875, China;

<sup>2</sup>Department of Atmospheric and Oceanic Sciences, School of Physics, Peking University, Beijing 100871, China

## Abstract

**Significance** Ozone is an important trace gas in the atmosphere and can affect the state and process of the troposphere and stratosphere. About 90% of ozone is concentrated in the stratosphere (10–50 km) and can absorb ultraviolet radiation from the sun, thus affecting the atmospheric circulation and the earth's climate, and protecting the earth's life system. 10% of ozone is located in the troposphere, which exerts an important influence on atmospheric chemistry, air quality, and climate change, and its spatial distribution is affected by both cross-regional transport and regional production. The main source of near-surface ozone is a photochemical reaction, and its main precursors are carbon monoxide (CO), nitrogen oxides ( $\text{NO}_x$ ), and volatile organic compounds (VOCs). In addition, near-surface ozone concentration is also affected by meteorological conditions and regional transport. In recent years, ozone has become the primary pollutant after PM<sub>2.5</sub> in China and even the world, especially in summer and autumn. Correspondingly, ozone pollution prevention and control have been the focus of air pollution control in the future.

Ozone data can be obtained by ground-based, sounding, airborne, and space-borne observations. The ground-based observation stations can provide spatial-temporal distribution information of ozone. The data at each site are of high accuracy and good stability with the insufficient spatial representation of the sites, and the ozone concentration in the whole troposphere is not well-reflected. The vertical distribution characteristics of atmospheric ozone can be obtained by sounding and airborne observations, which can be employed to verify the satellite observation accuracy. However, the lack of spatial-temporal continuity makes it difficult to obtain the ozone distribution in a large area. As space-borne observations are not subject to geographical restrictions, it is possible to acquire global ozone spatial-temporal distribution information with all-weather coverage and provide hyperspectral and high-precision data. Therefore, high-precision, global, and all-weather ozone information can be obtained based on multiple satellite detection payloads.

**Progress** Currently, the global ozone detection instruments are divided into three detection methods of nadir observation, occultation observation, and limb-viewing (Fig. 1). The total ozone column with high precision and ozone profiles with low vertical resolution can be obtained by the nadir observation. The ozone profile can be detected by limb-viewing and occultation observation. Occultation observation features high vertical resolution and precision, but with limited sampling frequency and small data volume. In contrast, limb-viewing can detect ultraviolet, infrared, and microwave bands, and it has high sampling frequency and can realize all-weather sampling. According to the detection spectrum and detection principles, global ozone detection instruments can be divided into ultraviolet spectral detection sensors and infrared spectral detection sensors. Based on the satellite development technologies, the inversion algorithms of the total ozone column and ozone profile are proposed (Figs. 3 and 4), and the estimation method of near-surface ozone is developed by integrating multi-source data. The whole layer ozone information and the vertical ozone distribution information can be obtained from the ultraviolet spectrum and infrared spectrum of satellites respectively. The monitoring accuracy of the total ozone column has currently reached 90%, but the inversion accuracy of the ozone concentration in the middle and lower troposphere and near the surface needs to be improved. According to the current level of inversion technology, the combination of various technical methods can be adopted to improve the detection capability of the middle and lower ozone.

The application of various ozone satellite remote sensing can be carried out in the technology of atmospheric ozone detection and inversion. Our study focuses on ozone pollution progress, including the analysis of spatial-temporal characteristics of ozone pollution and typical pollution events, and the interaction between ozone pollution and meteorological conditions. The different meteorological factors can affect ozone pollution precursors. Quantifying the influence of meteorological conditions on the photochemical reaction process of ozone is an important prerequisite for formulating scientific emission reduction schemes to improve air quality. The analysis of typical ozone pollution processes can clarify the formation mechanism, development process, and subsequent evolution of near-surface ozone pollution.

**Conclusions and Prospects** The continuous development of instrument design and inversion technology of various satellite detection payloads makes it possible for satellite remote sensing inversion and monitoring applications of ozone. The supervision and control of ozone pollution need to find out the source and accurately evaluate the pollution cases,

which can be gradually analyzed in precursor emissions, chemical conversion, meteorological influence, and three-dimensional transport. The synergistic emission reduction of VOC<sub>s</sub> and NO<sub>x</sub> is the ozone treatment fundamental in China, and it is also the major research direction in the next step.

**Key words** atmospheric optics; ozone; satellite remote sensing; inversion algorithm; precision validation; air quality; stratospheric intrusion